Geomorphology 394 (2021) 107950

Contents lists available at ScienceDirect

Geomorphology

journal homepage: www.elsevier.com/locate/geomorph

3D morphology of a glacially overdeepened trough controlled by underlying bedrock geology

Lukas Gegg [a,*], Gaudenz Deplazes [b], Lorenz Keller [c], Herfried Madritsch [b], Thomas Spillmann [b], Flavio S. Anselmetti [a], Marius W. Buechi [a]

[a] Institute of Geological Sciences and Oeschger Centre for Climate Change Research, University of Bern, Baltzerstrasse 1+3, 3012 Bern, Switzerland
[b] National Cooperative for the Disposal of Radioactive Waste (Nagra), Hardstrasse 73, 5430 Wettingen, Switzerland
[c] roXplore gmbh, Oberfeldstrasse 6, 8514 Amlikon-Bissegg, Switzerland

ARTICLE INFO

Article history:
Received 15 April 2021
Received in revised form 21 July 2021
Accepted 13 September 2021
Available online 15 September 2021

Keywords:
Subglacial erosion
Overdeepening
Trough morphology
Surface seismics

ABSTRACT

Subglacial overdeepenings are common elements of mountain forelands and have considerable implications for human infrastructure. Yet, the processes of overdeepening by subglacial erosion and especially the role of bedrock geology are poorly understood. We present a case study of the Gebenstorf-Stilli Trough in northern Switzerland, a foreland overdeepening with a regionally unique, complex underlying bedrock geology: in contrast to other Swiss foreland overdeepenings, it is incised not only into Cenozoic Molasse deposits, but also into the underlying Mesozoic bedrock. In order to constrain the trough morphology in 3D, it was targeted with scientific boreholes as well as with seismic measurements acquired through analysis of surface waves. Our results reveal an unexpectedly complex trough morphology that appears to be closely related to the bedrock geology. Two sub-basins are incised into calcareous marls and Molasse deposits, and are separated by a distinct ridge of Jurassic limestones, indicating strong lithological control on erosional efficiency. We infer generally relatively low glacial erosion efficiency sensu stricto (i.e. quarrying and abrasion) and suggest that the glacier's basal drainage system may have been the main driver of subglacial erosion of the Gebenstorf-Stilli Trough.

1. Introduction

Subglacial overdeepenings, i.e. closed troughs eroded below the fluvial base level, are common elements of formerly glaciated mountain forelands (Cook and Swift, 2012). In the northern European Alpine example, they underlie ~10% of the land surface (Dürst Stucki and Schlunegger, 2013). Despite their significance for, among others, construction projects, groundwater and radioactive waste disposal (Preusser et al., 2010; Stumm, 2010), the understanding of overdeepenings in terms of formation processes and controlling factors is limited and subject to debate (Cook and Swift, 2012; Alley et al., 2019). This applies especially to the influence of bedrock geology on the efficiency of subglacial erosion (Goudie, 2016).

Several authors (e.g. Augustinus, 1992; Brook et al., 2004) have reported a correlation of rock mass strength and glacial trough cross section, with steep and narrow troughs developing in resistant bedrock, and wide and shallow troughs in weak lithologies. However, effects of more complex patterns of bedrock lithology have hardly been studied. As an exception, Pomper et al. (2017) reported deeper-reaching subglacial erosion where the Lower Salzach Valley (Austria) is underlain by soft Cretaceous marls as opposed to lime- and dolostones. Further, Harbor (1995) modelled glacial erosion into bedrock with a weak zone in the trough centre, and observed increased downcutting, narrowing and steepening initiating in but, not restricted to, the weak zone. On a smaller scale, Glasser et al. (1998) showed by detailed field mapping that discontinuities from bedrock foliation parallel to the ice flow enhance erosion through quarrying, whereas discontinuities orthogonal to ice flow rather increase abrasion. Similarly, the orientation of sedimentary bedding has a discernible influence on basal ice velocity and thus on subglacial landform morphology (Phillips et al., 2010). Quarrying is frequently considered the more efficient glacial erosion process (e.g. Cohen et al., 2006; Zoet et al., 2013; Alley et al., 2019), but in weak and poorly jointed rocks, abrasion might outweigh quarrying (Krabbendam and Glasser, 2011). The importance of jointing and joint spacing has been further highlighted by Dühnforth et al. (2010), who found a strong correlation of glacial erosion rates and fracture density (see also Hooyer et al., 2012; Becker et al., 2014). Most of these investigations specifically focused on glacial erosion in non-overdeepened settings.

In overdeepenings, characterized by an adverse slope at the distal end, the subglacial hydrological conditions are very different (Cook and Swift, 2012). In order to maintain erosion, sediment has to be evacuated from the glacier base against this adverse slope, whereby

* Corresponding author.
E-mail address: lukas.gegg@geo.unibe.ch (L. Gegg).

https://doi.org/10.1016/j.geomorph.2021.107950

pressurized melt water plays an important role (Alley et al., 1997, 2019; Cook and Swift, 2012; Buechi et al., 2017). The abundance of subglacial water steadily increases towards the glacier snout, where it facilitates the erosion of large terminal overdeepenings even under diffluent ice (Herman et al., 2011). There, subglacial water has been suggested to be the main driver of subglacial erosion, analogous to tunnel valleys (Cofaigh, 1996); Dürst Stucki et al., 2010; Fiore et al., 2011; Dürst Stucki and Schlunegger, 2013). It is therefore questionable to what extent the findings of subglacial erosion in non-overdeepened settings can be applied to the formation and evolution of overdeepened glacial troughs.

This study sheds light on the morphology of a subglacial overdeepening in the northern Alpine foreland of Switzerland, based on borehole and seismic data. The selected overdeepening is of special interest and relevance due to its unique, complex bedrock geology. The connection of the trough morphology with bedrock architecture and the area's tectonic setting allow inferences about the geological controls and the processes of overdeepening erosion.

2. Study area

The study area is located in northern Switzerland, close to the eastern termination of the WSW-ENE trending Jura Mountains (Fig. 1). The local bedrock stratigraphy comprises Triassic and Jurassic sediments deposited on an epicontinental platform and unconformably overlain by Cenozoic clastics of the northern Alpine Molasse Basin (Bitterli-Dreher et al., 2007; Jordan et al., 2008).

The oldest rocks exposed at the surface of the study area are shallow marine limestones and dolomites of the Schinznach Formation (Fm.; late Middle Triassic; Figs. 2A, A.1). They are overlain by the Middle to Late Triassic Bänkerjoch Fm., an alternation of gypsum/anhydrite with claystone and dolomite, and Klettgau Fm., a heterogeneous unit comprising mostly marl, silt- and sandstone. The following Early Jurassic Staffelegg Fm. as well as the Opalinus Clay of the early Middle Jurassic consist of marine claystones, siltstones and marls. During the later Middle Jurassic, marls and limestones (PKI: Passwang Fm., Klingnau

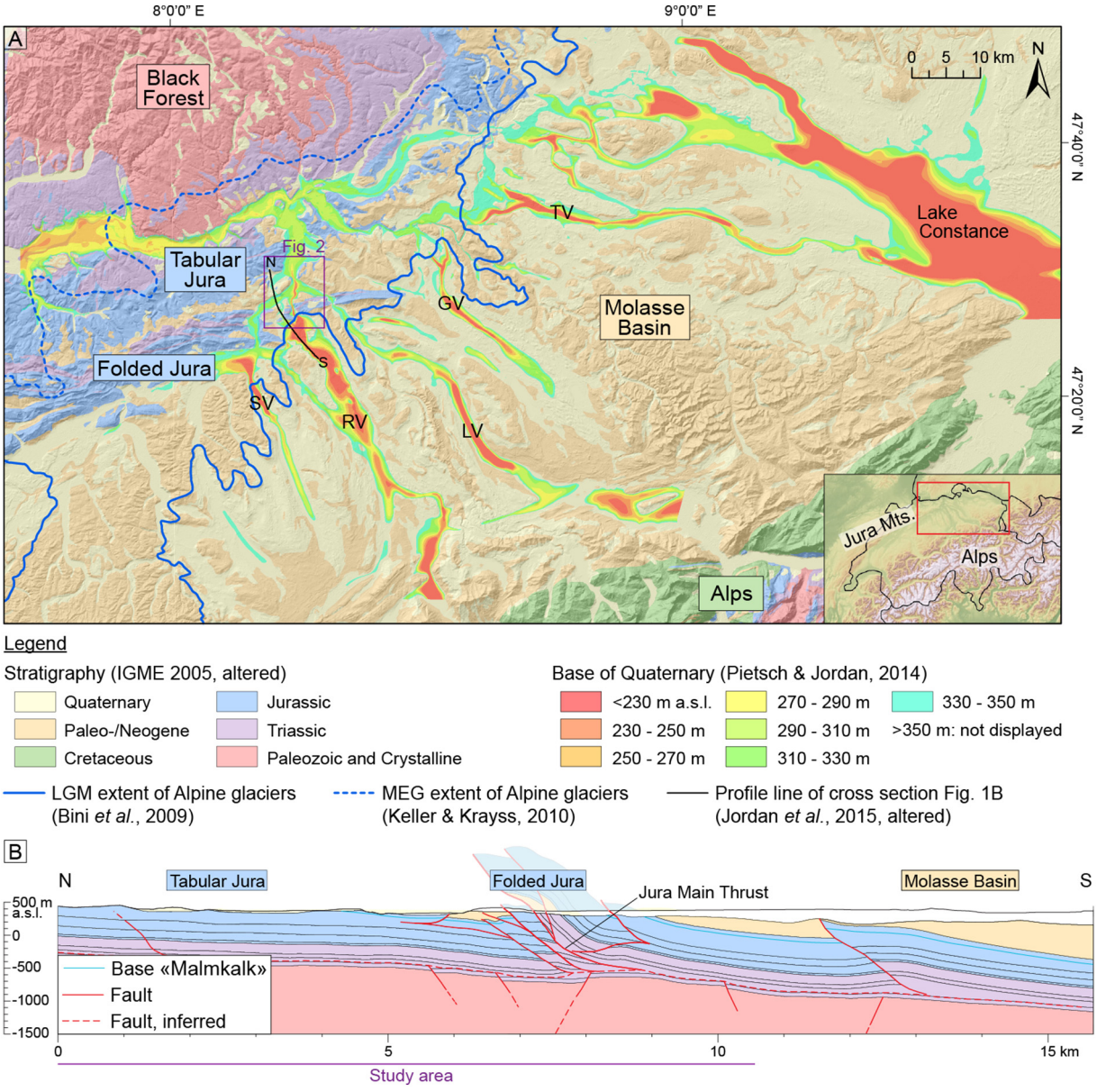

Fig. 1. Overview map of central and eastern northern Switzerland with major tectonic units and surface geology (A; IGME 2005: Commission for the Geological Map of the World et al., 2005; LGM: Last Glacial Maximum; MEG: Most Extensive Glaciation). The cross-section on B (from Jordan et al., 2015, altered) illustrates the tectonic architecture of the study area (purple box in A). Note that foreland overdeepenings (SV: Seetal Valley, RV: Reuss Valley, LV: Limmat Valley, GV: Glatt Valley, TV: Thur Valley) generally only occur within the Molasse basin, with the exception of the Gebenstorf-Stilli Trough (Fig. 2).

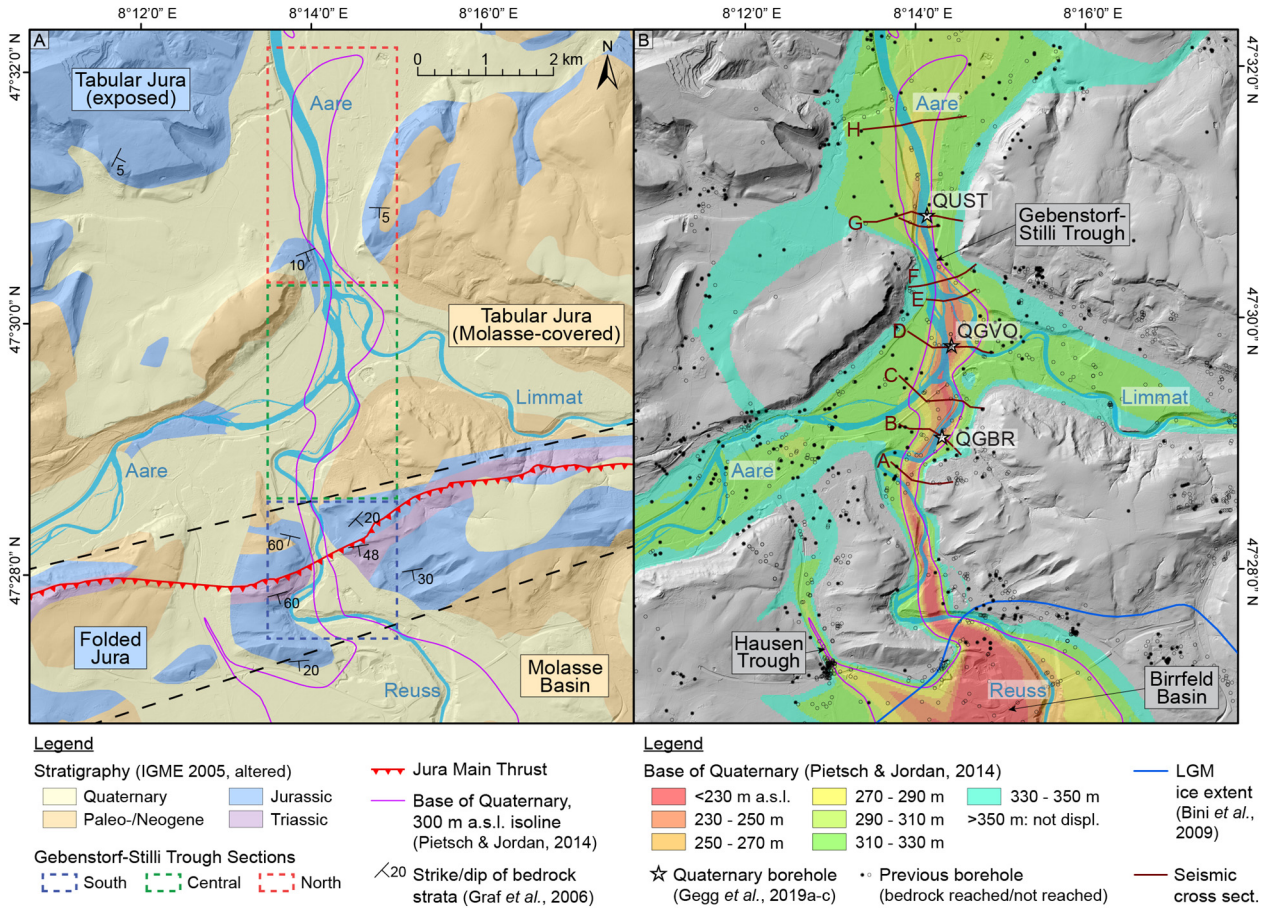

Fig. 2. Overview map of the Gebenstorf-Stilli Trough. A: Simplified surface geology. B: Locations of boreholes and acquisition lines of seismic cross sections. For localization, please refer to Fig. 1.

Fm., Ifenthal Fm.; Fig. A.1) were deposited in a shallow sea that deepened towards the early Late Jurassic, when the predominantly calcareous marls of the Wildegg Fm. formed (Gygi, 2000; Deplazes et al., 2013). These marls transition gradually over few meters to decameters into bedded and massive marine limestones of the Villigen and Burghorn Fms. (in the following referred to as «Malmkalk»; Fig. A.1; Gygi, 2000; Bitterli-Dreher et al., 2007; Jordan et al., 2008).

In the Paleogene, the Mesozoic strata of the Jura Mountains were uplifted on the forebulge of the Alpine orogeny and began being eroded and karstified, while further south/southeast the Molasse Basin subsided (Fig. 1; Pfiffner, 1986; Berger et al., 2005). In Oligocene-Miocene times heterogeneous sandstones, siltstones, and marls of the Lower Freshwater, Upper Marine, and Upper Freshwater Molasse were deposited in the study area, and generally remained rather poorly lithified (Fig. A.1; Bitterli-Dreher et al., 2007). The Molasse deposition ended in the Late Miocene, around the same time the Folded Jura (FJ) formed. It was upthrusted as a consequence of collisional tectonics in the Central Alps via thin-skinned deformation above an evaporitic décollement horizon within Middle to Upper Triassic evaporites (Laubscher, 1962; Burkhard, 1990). This décollement horizon crops out along the Jura Main Thrust that formed between 9 and 4 Ma (Fig. 1B, 2A, 2; Looser et al., 2021). The Mesozoic sequences south of it, i.e. within its hanging wall, are affected by a dense stack of thrusts and dip moderately towards the south (Fig. 2A; Malz et al., 2015). By contrast, north of the Jura Main Thrust the Mesozoic strata dip only very gently southward (Tabular Jura: TJ; Fig. 2A). While the Mesozoic is overlain by a wedge of Molasse deposits immediately north of the Jura Main Thrust, continuously older rocks are exposed further to the north, where they form plateaus (e.g. in the northwest of Fig. 2).

During the Pleistocene, multiple advances of Alpine glaciers reached far into the foreland and considerably reshaped the landscape (Graf, 2009; Keller and Krayss, 2010; Preusser et al., 2011). This includes the subglacial erosion of overdeepenings, most of which are carved exclusively into Molasse deposits (Fig. 1; Graf, 2009; Preusser et al., 2010). An exception is the Gebenstorf-Stilli Trough (GST), which cuts through the FJ and into the TJ (Fig. 2; Jordan, 2010). It extends ~9 km northward from the Birrfeld Basin (Nitsche et al., 2001) into the present-day confluence area of the rivers Aare, Reuss and Limmat and has a distinctly elongated shape with a maximum width of ~1 km (enclosed by the 300 m a.s.l. isoline; Bitterli-Dreher et al., 2007; Pietsch and Jordan, 2014). The maximum trough depth exceeds 110 m below surface and 75 m below the lowest known Pleistocene base level (PBL, 300 m a.s.l.; Graf, 2009; Gegg et al., 2020). Situated entirely outside the LGM (Bini et al., 2009), the GST was presumably incised during the late Middle Pleistocene (Bitterli-Dreher et al., 2007; Graf, 2009). The significant narrowing from the wide Birrfeld basin towards the GST coincides with a change in trough morphology from U-shaped to V-shaped (Jordan, 2010; Dürst Stucki and Schlunegger, 2013). It has been hypothesized that the narrowing and change in shape are a result of the dominant bedrock lithology changing from rather soft, poorly lithified Molasse sandstones, siltstones and marls in the south towards the more resistant limestones and marls of the Jura Mountains in the north (Bitterli-Dreher et al., 2007; Jordan, 2010).

3. Methodology

The Gebenstorf-Stilli Trough was investigated with three scientific boreholes along its trough axis (Fig. 2B). These are, from south to

north, QGBR (47°29′00″ N, 8°14′11″ E; Gegg et al., 2019b), QGVO (47°29′43″ N, 8°14′18 E; Gegg et al., 2019c), and QUST (47°30′46″ N, 8°14′3″ E; Gegg et al., 2019a). All three boreholes terminated at least 10 m into the bedrock to allow for a confident bedrock identification. Recovery and core quality were maximized by combined application of pneumatic hammering ('Düsterloh Hammer') and wire-line drilling with a triple-tube core barrel. After detailed stratigraphic logging of the drill cores, selected 1-m-intervals were sampled for petrographic analysis of coarse-grained sediments (>100 clasts >15 mm in diameter, if not indicated otherwise).

To further constrain the morphology of the Gebenstorf-Stilli Trough, we recorded ambient noise on ~230 seismic 3-component stations that were distributed along eight acquisition lines (Fig. 2B; (Nagra, 2021). The data processing workflow is sketched on Fig. 3 and involved computation of the horizontal-to-vertical spectral ratio (HVSR) for each of the 10–30 min long recordings and picking of the respective fundamental frequency f_0 (Fig. 3A; SESAME European Research Project, 2004). The frequency of the pulse maximum f_0 depends on the depth of the shear wave (S-wave) velocity contrast indicative for the bedrock below unconsolidated sediments. In case of ambiguity in the spectral information, f_0 was selected conservatively, with regard to the bedrock model of Pietsch and Jordan (2014).

Conversion of f_0 to bedrock depth z is possible if the average S-wave velocity of the Quaternary strata $v_{s,E}$ is known (Eq. (i); see Nakamura,

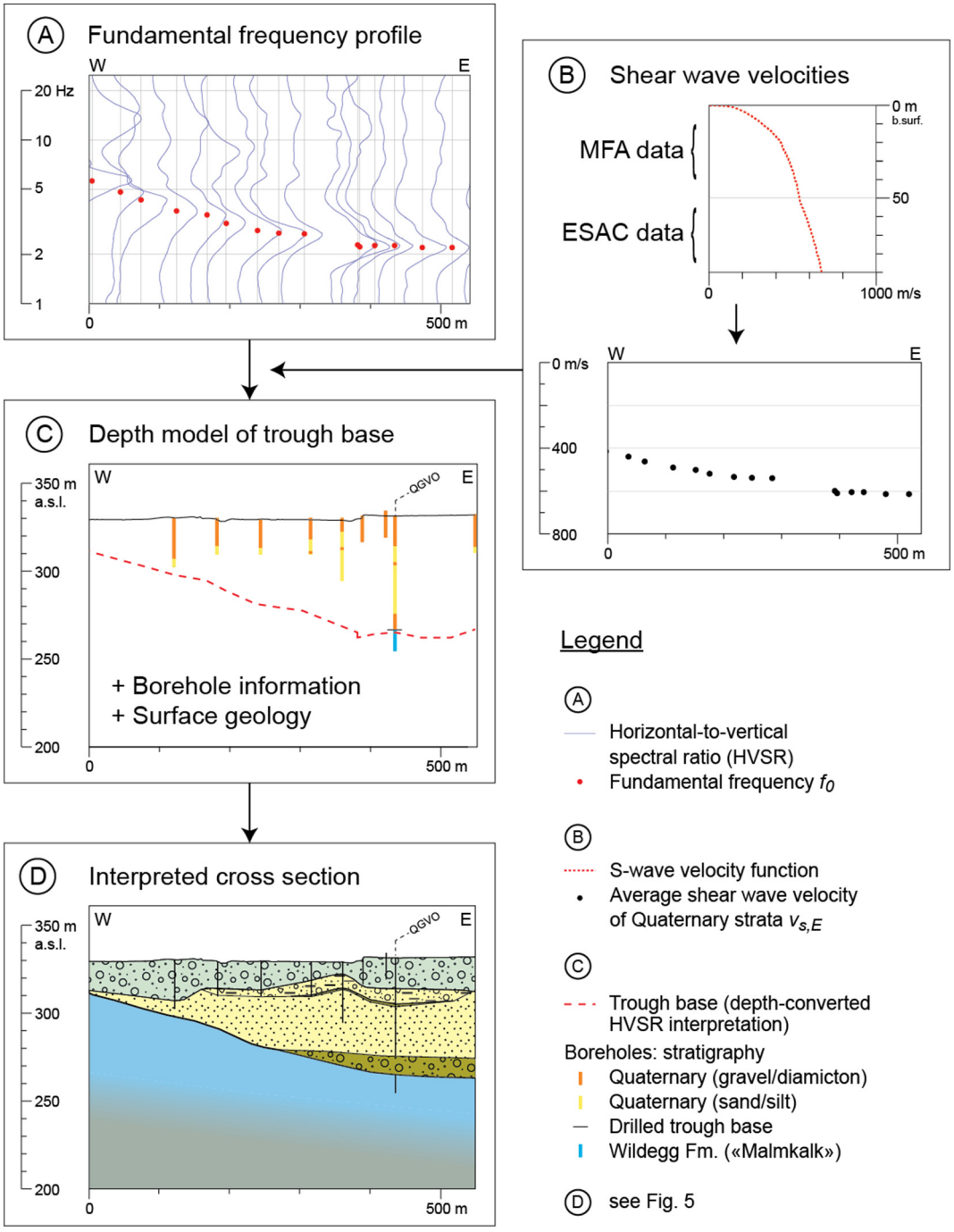

Fig. 3. Workflow applied for the construction of the cross sections from the geophysical data exemplified by a clip of acquisition line D. The fundamental frequency profile (A) is, with help of the shear wave velocity profile (B), converted into a depth model of the trough base (C), and complemented with borehole and surface data to a finalized geological cross section (D).

1989 for details). It was determined by joint inversion of ~50 active measurements after Dziewonski et al. (1969; multiple frequency analysis MFA) in combination with deeper reaching ESAC measurements (extended spatial auto correlation; Ohori et al., 2002; typically one measurement per acquisition line) following Dal Moro et al. (2018). This process provided one S-wave velocity function per line, which was windowed for the intra-Quaternary part (S-wave velocity < 1100 m/s; Wiemer et al., 2016) and averaged to obtain location-specific $v_{s,E}$ values (Fig. 3B). These were applied to Eq. (i) for conversion of f_0 into depth profiles of the base of Quaternary (Fig. 3C, D).

$$z = {}^{v_{s,E}}\!/_{4*f_0} \quad \text{(i)}$$

We base our study on a geological and morphological interpretation of the resulting cross sections integrating surface (1: 25′000 geological map: Graf et al., 2006; 2 m LiDAR DEM: Swisstopo, 2013) and subsurface information (drill logs from the borehole database of the Swiss Cooperative for the Disposal of Radioactive Waste (Nagra); previous 25 m base of Quaternary DEM: Pietsch and Jordan, 2014). For cross section construction, boreholes with a distance of max. 200 m from the respective acquisition line were projected parallel to the isolines of the Gebenstorf-Stilli Trough by Pietsch and Jordan (2014). The base of Quaternary was fitted to the boreholes while maintaining the seismically determined trough shape. Interpretations are focused on the overdeepened part of the trough, i.e. that lying below PBL at ~300 m a.s.l. (Graf, 2009). The same applies to the V-index (VI; Zimmer and Gabet, 2018) as a quantifier of trough shape. A perfectly V-shaped trough with even flanks would be characterized by a VI of 0, whereas increasing values correspond to more concave flanks, i.e. an increasingly U-shaped cross section.

4. Results

4.1. Planform morphology

In terms of bedrock geology, the GST can be subdivided into three sections of approximately equal length. The southern section is embedded in the Folded Jura (FJ), whereas the middle section is mostly incised into Molasse deposits, and the northern section into the Mesozoic of the Tabular Jura (TJ, Fig. 2A). These three sections show striking differences in planform morphology (Pietsch and Jordan, 2014): both the TJ and FJ sections are narrow (300–400 m at 300 m a.s.l) and either straight in their entirety or composed of straight segments, respectively. In contrast, in the Molasse section the trough takes a sinuous course towards north while widening gradually (up to ~800 m at 300 m a.s.l.) until a sudden constriction at the transition to the TJ. The sinuosity index S of the Molasse section, defined as the ratio between total length of the trough axis between two selected points and the shortest connection of said points, is 1.06 (Fig. C.1). Our boreholes and seismic acquisition lines cover the central (QGBR, QGVO, lines A–E) and northern (QUST, lines F–H) sections of the GST (Fig. 2B).

4.2. Boreholes

QGBR and QGVO recovered Late Pleistocene Niederterrasse gravels overlying a thick unit of lacustrine/deltaic sand and several meters of basal coarse-grained sediment, while the trough infill in QUST almost exclusively comprises gravels (Fig. 4; see Fig. 2B for locations). The coarse-grained deposits consist largely of far-travelled, i.e. Alpine or Molasse-derived, clast lithologies dominated by grey limestones, diverse sandstones, and quartzites (Fig. 4). Lithologies of the local Jura Mountains play a subordinate role: light beige limestone clasts that can be attributed to the Villigen Fm. («Malmkalk») make up no more than 18% (usually below 10%), and calcareous marl clasts attributed to the Wildegg Fm. were not encountered in the chosen intervals. Only the lowermost ~0.3 m of the Quaternary infill at QGBR consists predominantly of light limestone fragments, and the lowermost ~0.4 m of QUST contains individual soft marly clumps identified as Wildegg Fm. (Gegg et al., 2019a, 2019b).

The boreholes reached the base of the overdeepening in depths of 111.5 m (225.8 m a.s.l.), 64.9 m (266.1 m a.s.l.), and 76.0 m (255.2 m a.s.l.), respectively (Fig. 4). Light beige limestones of the «Malmkalk» were encountered below the overdeepening in QGBR and QGVO, and grey calcareous marls of the Effingen Member, Wildegg Fm., in QUST. We combined these findings with the logs of >450 existing boreholes in the perimeter as well as a 1:25′000 scale geological map (Graf et al., 2006) to a base Quaternary subcrop map (see Section 5.2). The generally massive «Malmkalk» is characterized by frequent stylolites in varying orientations including horizontal and vertical, as well as shallow (<40°), southeast-dipping fractures with an average spacing of ~0.6 m in QGBR, and ~1.4 m in QGVO (corrected after Terzaghi, 1965). Deep-reaching, sediment-filled paleokarst predating the Quaternary and exhibiting presumed subglacial hydrofractures was encountered in QGBR (Gegg et al., 2020). The calcareous marls of the Wildegg Fm. have a similar fracture spacing of ~1.1 m in QUST, and contain intervals where the rock is softened or granular-disintegrating. The bedrock surface is truncated by a karst cavity in QGBR, but developed as a sharp, horizontal boundary in QGVO and QUST with minor drilling-induced disturbance by fresh fracturing and/or grinding.

4.3. Surface-seismic sections

The interpreted cross sections are plotted on Figs. 5, and B.1–B.8 show the individual cross sections together with the respective raw data. The uncertainty of the applied method is difficult to quantify as it depends on multiple factors, such as the heterogeneity of the trough infill, the local inclination of the base of Quaternary, the impedance contrast to the bedrock, the presence of other geological boundaries (e.g. Molasse-Mesozoic) in close proximity, and the amplitude and frequency of industrial noise. Empirically, the seismic measurements are in good accordance with boreholes in the vicinity (max. Distance 170 m). Average differences amount to −7/+10 m, with maximum values of −21/+22 m (over- and underestimation, respectively; see Table B.1). An exception is the site of borehole QGBR, where the trough depth is underestimated by ~30 m, however this borehole is located close to the trough wall that has likely affected the respective measurements (Table B.1, Fig. 5). The intra-Quaternary shear wave velocities show an increasing trend towards the north (~500 m/s at 50 m depth for lines A and B, ~550 m/s for lines C and D; ~600 m/s for line G). Although these differences are smaller than the variations along a given line, they correlate with a trough infill that becomes increasingly more coarse-grained and higher in density towards the north (Fig. 4; Gegg et al., 2019a, 2019b, 2019c).

The cross sections show a trough composed of two sub-basins (Gebenstorf Basin in the central and Stilli Basin in the northern trough section; 'nested basins' after Patton et al., 2016) separated by a distinct bedrock ridge (Lauffohr Ridge, Figs. 5, 6). The GST gradually widens from ~350 to ~800 m at 300 m a.s.l. (i.e. at PBL; Graf, 2009) between lines A and D while transitioning from a V- to a more U-shaped cross section (VI increases from 0.2 to 0.4). This widening coincides with a shallowing of the overdeepened centre from its maximum depth at ~225 to ~265 m a.s.l., following the trend of the «Malmkalk» surface that rises towards the TJ (Fig. 6), and as a result, the overdeepened cross sectional area remains approximately constant (Fig. 5). North of line D, the trough narrows abruptly and further shallows to ~295 m a.s.l. at line E, where the bedrock geology changes gradually from «Malmkalk» to the underlying marl (Wildegg Fm.; Fig. 5). Further north (lines F–H), seismic data are afflicted by greater uncertainties than in the south. The trough deepens to at least 255 m a.s.l. at QUST, and the distinct trough shoulder east of QUST (constrained by a second borehole on line G, Figs. 5, B.7) suggests a rather U-shaped cross section

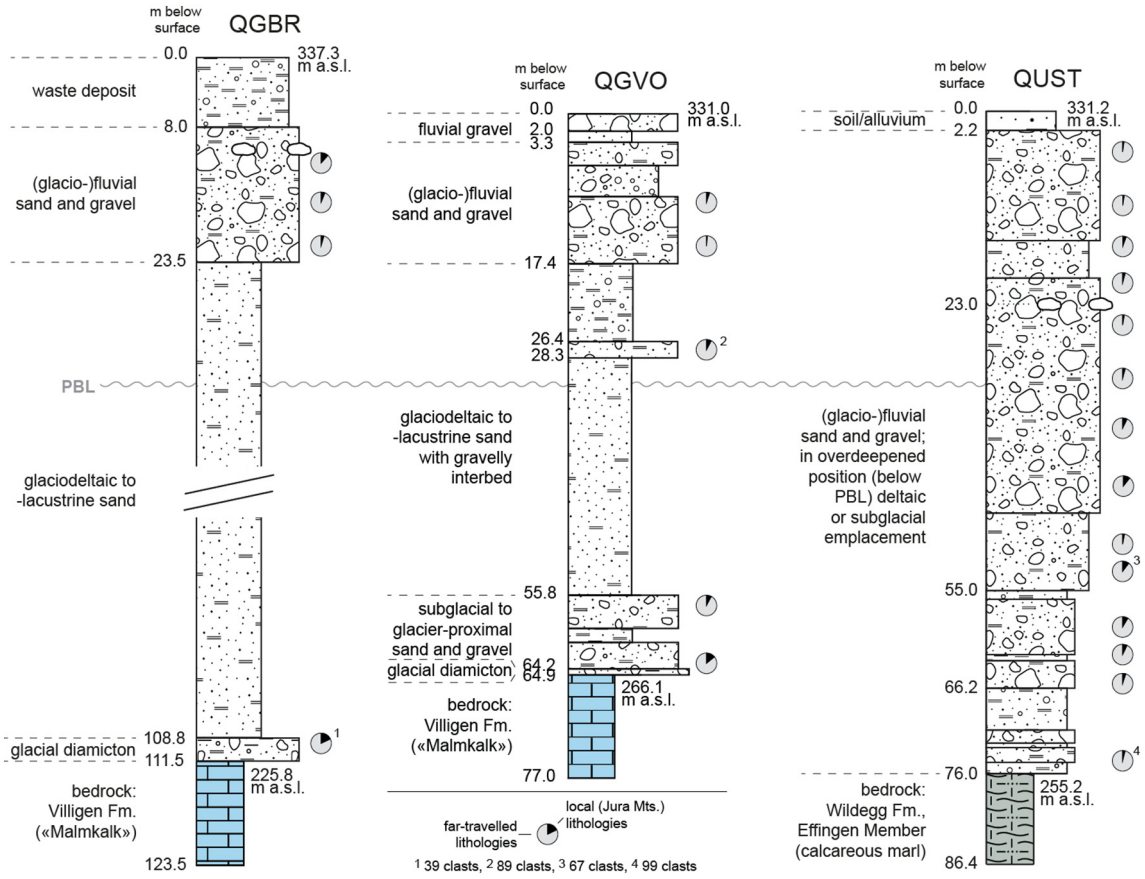

Fig. 4. Lithological logs of Quaternary boreholes QGBR, QGVO, and QUST (from Gegg et al., 2019a, 2019b, 2019c, altered). PBL marks the lowest known Pleistocene base level at ~300 m a.s.l. (Graf, 2009). Pie charts show the ratio of local limestones vs. far-travelled clasts in coarse-grained sediments (>100 clasts >15 mm, if not indicated otherwise).

(VI = 0.6). The overdeepening terminates close to line H, with an average adverse slope of ~1.6° between lines G and H (Fig. 6).

5. Discussion

5.1. Planform morphology

5.1.1. Paleo-ice flow and erosion

Dürst Stucki and Schlunegger (2013) distinguish two general types of overdeepenings in the vicinity of the Alps, i) proximal Alpine-type overdeepenings composed of straight segments, and ii) distal, anastomosing foreland-type overdeepenings (see also Magrani et al., 2020). These morphologies are interpreted as a result of geological as well as paleo-glaciological differences: while Alpine-type overdeepenings are carved into zones of weakness (i.e. fault zones) by thick ice streams in the mountain valleys, foreland-type overdeepenings occur in the generally rather poorly lithified Molasse deposits independently from structural weak zones (Preusser et al., 2010; Dürst Stucki and Schlunegger, 2013). Pressurized subglacial melt water plays an important role especially in the erosion of foreland overdeepenings near the glacier termini (Herman et al., 2011; Alley et al., 2019), and could possibly be its main driver (Dürst Stucki et al., 2010; Dürst Stucki and Schlunegger, 2013).Morphologically, the central section of the GST resembles a typical foreland overdeepening, whereas the southern (FJ) and northern (TJ) sections have more similarities with inner-Alpine overdeepenings. This morphological variability occurs despite the common distal position, similar melt water availability (periodically high) and ice thickness (low), suggesting the same prevailing erosional mechanisms (see Section 5.2.2; Herman et al., 2011; Cook and Swift, 2012). We infer that in the case of the GST, the morphological differences are controlled predominantly by the bedrock geology and resulting pre-glacial topography.

The Mesozoic strata outcropping in the FJ and TJ have a higher bulk erosional resistance than the Molasse deposits (Kühni and Pfiffner, 2001) despite strong internal variations (Yanites et al., 2017) and it has been shown before that glacial troughs tend to be narrower in more resilient rocks (Augustinus, 1992; Brook et al., 2004). In addition, the erosional resistance of the Mesozoic has facilitated the Jura Mountains to persist as a low mountain range for several millions of years, whereas the Molasse Basin topography is comparatively levelled off. As a consequence, while Pleistocene ice flow over Molasse deposits could diverge to the sides, the FJ and TJ sections of the GST lie within distinct, likely pre-existing valleys (Ziegler and Fraefel, 2009). These valleys constrained the ice and basal water flow, which is often accompanied by an increase in velocity and erosional activity (Hallet, 1979; Herman et al., 2015; Patton et al., 2016). Given the similar trough widths in FJ and TJ, it appears that the different tectonic histories of both units are not expressed through significantly different erosional susceptibilities, which could be due to the structural strike of the FJ being orthogonal to paleo-ice flow (Glasser et al., 1998).

Although comparatively poorly constrained, the width of the overdeepened (below 300 m a.s.l.) GST appears to remain largely constant across the FJ (Fig. 1; Bitterli-Dreher et al., 2007; Pietsch and Jordan, 2014) where bedrock properties change drastically over short distances (Yanites et al., 2017). In contrast to the modern valley, the shape of the buried overdeepening is seemingly little affected by short-scale variations in erosional resistance, which applies also to the Hausen Trough further west (Fig. 2B; Graf, 2009; Pietsch and Jordan, 2014). This suggests that there is a certain inertia in trough morphology,

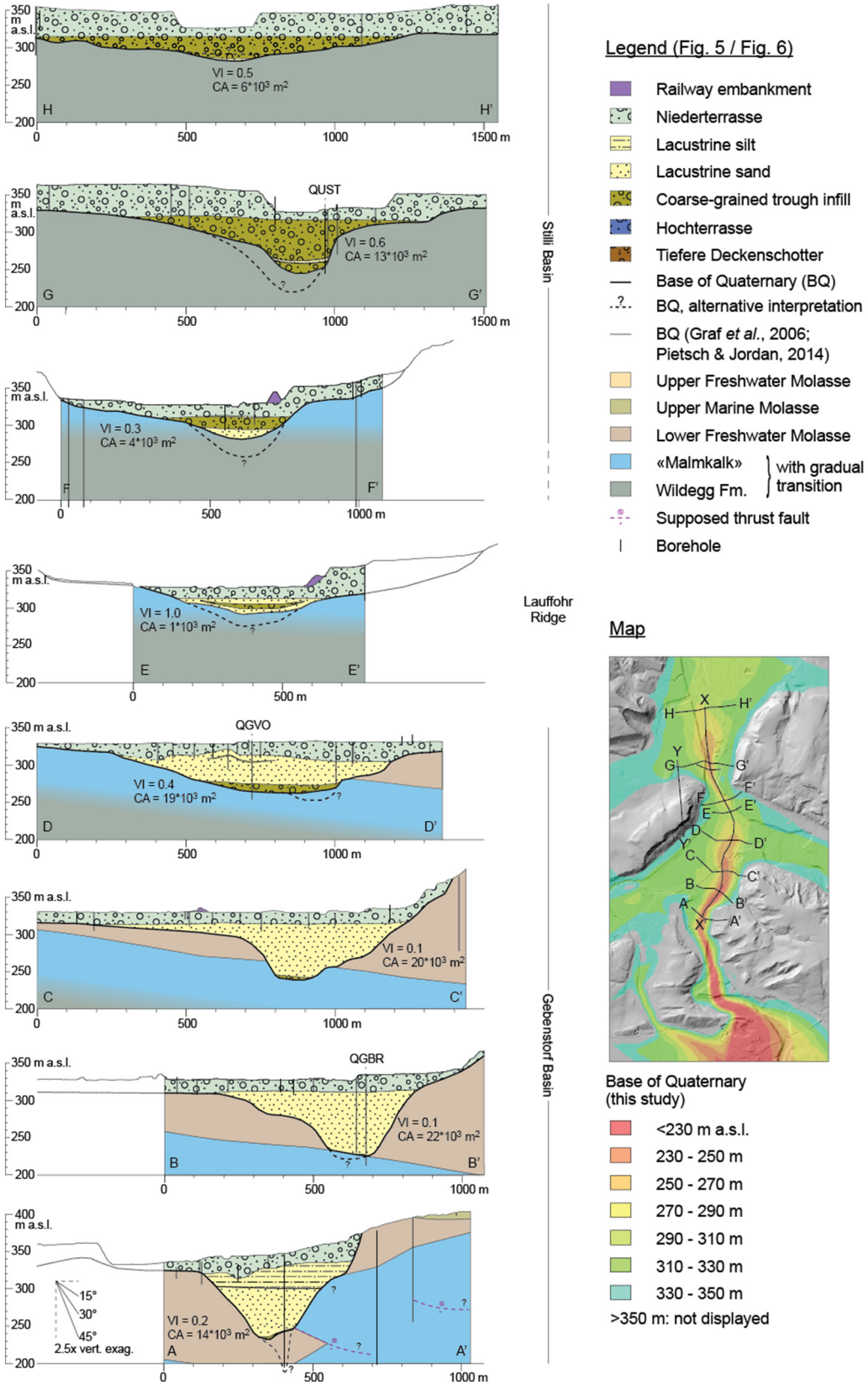

Fig. 5. Interpreted surface-seismic cross sections A-H (see also Figs. B.1–B.8). For location of the cross sections, see inset map or Fig. 2B. Profile traces X and Y refer to Fig. 6. VI = V-index (Zimmer and Gabet, 2018), CA = overdeepened cross sectional area (below 300 m a.s.l.).

which can adjust only gradually to bedrock changes. This hypothesis is supported by the slow and gentle widening of the GST after the transition from the FJ into the northward adjacent Molasse. As a result, the GST remains comparatively narrow even in its central section, with a maximum width that is more typical of inner-Alpine than for foreland overdeepenings (Table 1).

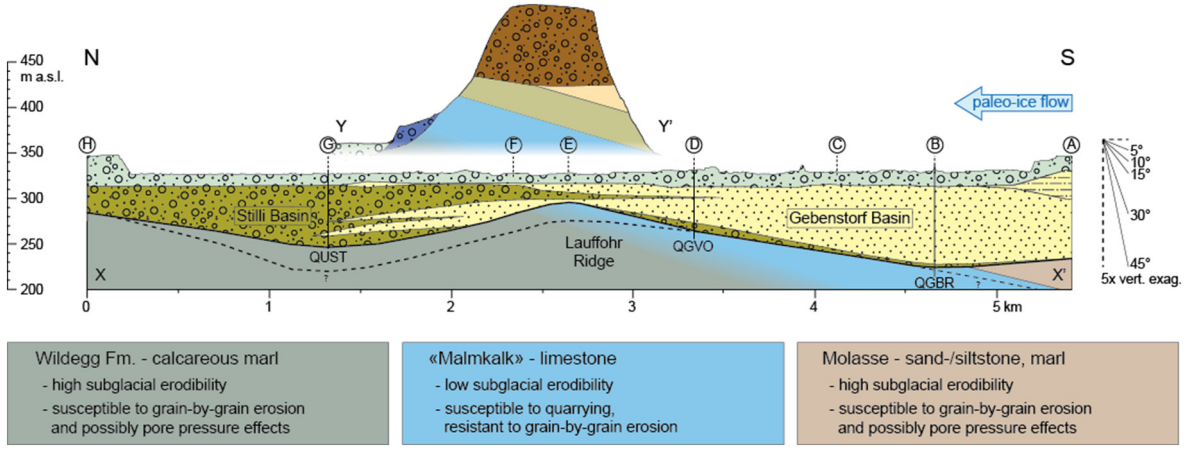

Fig. 6. Longitudinal section X of the Gebenstorf-Stilli Trough compiling cross sections A to H. Section Y through the Tabular Jura escarpment illustrates the dip of the bedrock strata. For localization and legend, please refer to Fig. 5. Relative erodibilities and presumed erosion processes of the relevant bedrock lithologies are summarized at the bottom (see Section 5.2.2).

5.1.2. The role of structural preconditioning

The Gebenstorf-Stilli Trough is the only known overdeepening of the northern Alpine foreland that extends significantly (i.e. kilometers) beyond the Molasse Basin (Fig. 1; Jordan, 2010), raising the question why such localized incision into the Mesozoic strata was possible at this specific position. Previously, structural geological control enabling the breach of the (fluvial) Aare Valley into the exposed TJ (approx. at line F) has been suggested (Haldimann et al., 1984). The straight and/or kinked morphology of those GST sections incised into Mesozoic bedrock support the idea that the overdeepening, and the likely preceding fluvial valley system (Ziegler and Fraefel, 2009), could follow discrete fault zones in the bedrock (similar to e.g. the inner-Alpine valleys of the rivers Rhone and Adda). This hypothesis is in the following reviewed based on our investigations.

At the outcrop-scale, N-S fractures, mostly with strike-slip kinematics, are a typical characteristic of Upper Jurassic limestones across the study area and beyond (Figs. 7, D.1; Madritsch, 2015). Minor N-S striking faults have been recognized in elongation of the GST (Matousek et al., 2000) and along strike of the FJ to the east (Diebold et al., 2006; Jordan et al., 2011). However, a densification of this kind of structures around the breach of the GST, especially in the TJ, is not discernable. In addition, individual strike-slip faults do not appear to have a strong structural imprint on the immediately surrounding Mesozoic bedrock (e.g. increase of fracture density, cataclasis development) according to field observations in the vicinity of the GST (Fig. D.1). No evidence for a major fault zone underneath the overdeepened trough has been observed in two regional seismic campaigns (Sprecher and Müller, 1986; Madritsch et al., 2013). However, the presence of a strike-slip fault zone with minor vertical throw hindering its seismic detection (Nagra, 2019) in the subsurface of the GST cannot be excluded. Despite the lack of evidence for a distinct fault zone, we can therefore not rule out structural control for the breach of FJ and TJ and/or glacial erosion thereafter.

In contrast to the southern and northern GST sections, the central section is characterized by a gently sinuous planform morphology. Its sinuosity (S = 1.06) is similar to other distal Molasse-hosted overdeepenings in the northern Alpine foreland (Pietsch and Jordan, 2014; Fig. C.1), e.g. Seetal Valley (S = 1.07), middle Reuss Valley (S = 1.05), Limmat Valley (S = 1.07), Glatt Valley (S = 1.12) and Thur Valley (S = 1.05), and generally similar to tunnel valleys (Cofaigh, 1996; van der Vegt et al., 2012). This morphology has previously been interpreted as indicative for erosion of the poorly lithified Molasse independent from structural control (i.e. not along straight fault segments; Preusser et al., 2010; Dürst Stucki and Schlunegger, 2013).

Table 1
Quantitative comparison of the Gebenstorf-Stilli Trough (GST) with other overdeepenings in Switzerland.
(Based on Magrani et al., 2020).

		Max. depth [m] below surface	Max width [m] 20 m below surf.*	Terminal adverse slope [°]
Alpine overdeepenings	Average	337	1453	2.7
	Median	288	962	1.7
Foreland overdeepenings	Average	180	2024	1.0
	Median	115	1298	0.6
Gebenstorf-Stilli Trough		≥112	920	1.6

* The approach by Magrani et al. (2020) uses a minimum sediment thickness or water column of 20 m to define overdeepening extent, thus maximum width is given 20 m below present-day ground surface.

5.2. Trough morphology in 3D

5.2.1. Lithological control on subglacial erosion

The maximum depth of the GST of ≥112 m below surface (~225 m a.s.l.) is typical for Swiss foreland overdeepenings (Table 1; Magrani et al., 2020). It is reached just beyond the FJ in the southern sub-basin (Gebenstorf Basin, GB) that shallows considerably further north. The shallowing of the GB occurs entirely within the narrow band of the «Malmkalk» that emerges at angle of ~4° towards the northwest, where it is exposed and referred to as TJ (Figs. 5, 6). This suggests strong lithological control for the depth of the basin: it appears that the subglacial erosional efficiency decreased significantly upon reaching the Jurassic limestones. A similar erosion pattern was observed in a seismic study of Lake Neuchâtel (NW Switzerland; Ndiaye et al., 2014), whose overdeepened floor reaches down to, but is not significantly incised into, the Mesozoic strata under ~200 m of Molasse cover. In QGBR, deep-reaching sediment-filled paleokarst was encountered in the limestone (Gegg et al., 2020). The fact that even karstified and presumably weakened «Malmkalk» was preserved and not completely eroded by the overdeepening glacier emphasizes its erosional resistance (see also Ndiaye et al., 2014). Moreover, the paleokarst walls throughout the bedrock interval of QGBR show abundant, randomly oriented surficial fractures, some of which are filled with intruded sediment (Gegg et al., 2020). The authors conclude that subglacial hydrofracturing is the most plausible explanation for the origin of these fractures, and that their abundance could point towards a multitude of subglacial water pressure events. Such a record would require erosion rates low enough to allow for prolonged direct contact of the karstified limestone with the glacier's basal drainage system. However, we consider possible

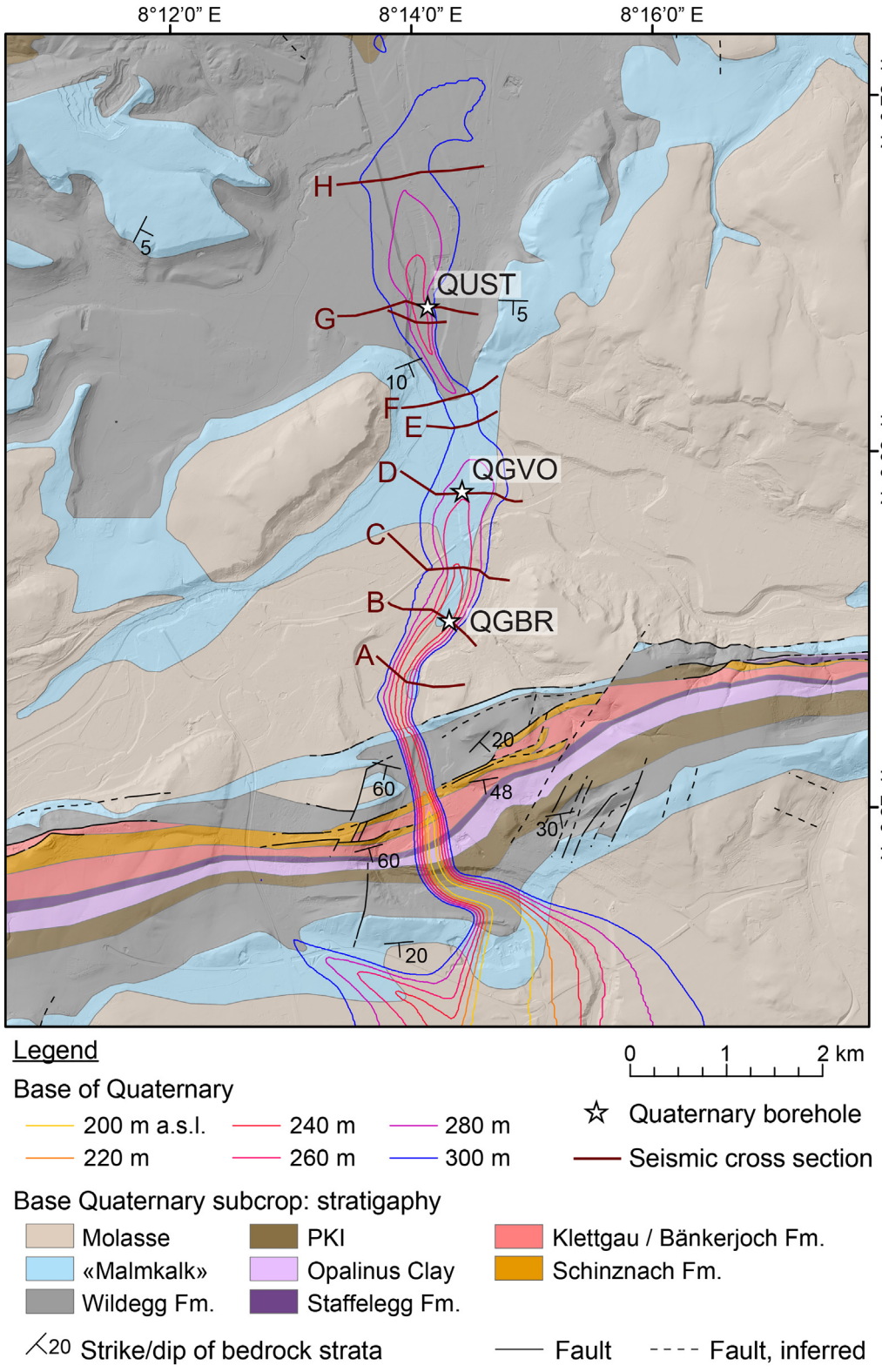

Fig. 7. Revised elevation model of the Gebenstorf-Stilli Trough (Loepfe et al., 2021) with underlying bedrock geology, combining surface geological information (Graf et al., 2006) with borehole data.

that the limited downcutting over the «Malmkalk» may have led to increased lateral erosion within the overlying Molasse, as the shallowing of the GB coincides with a doubling in trough width, so that the overdeepened cross sectional area remains nearly constant (see Fig. 5, sections A–D).

The shallowest depth of the GST is reached at the crest of the Lauffohr Ridge, where the base of the southward-dipping Jurassic limestone is breached (Figs. 6, 7). There, the GST is barely overdeepened as its base is close to PBL at 300 m a.s.l. (Graf, 2009). In the underlying calcareous marls of the Wildegg Fm. erosional efficiency was again

increased and culminated in the Stilli Basin (SB). We hypothesize that the enhanced erosion rates are the result of an interplay of several paleoglaciological as well as geological factors. Firstly, an abrupt increase in ice and melt water flux have likely increased subglacial erosion at the confluence of the catchments of Aare, Reuss, and Limmat (cf. MacGregor et al., 2000; Pomper et al., 2017). According to Ziegler and Fraefel (2009), this confluence had been established before, and remained largely fixed throughout, the Pleistocene. The deepening of the GST into the SB initiates where the three present-day valleys merge (Fig. 7), and it is not unlikely that a major ice confluence occurred at the same position during excavation of the GST. This position lies along the escarpment of the TJ (Figs. 6, 7), an area of increased topography, where ice flow was again focused into a morphologically defined valley, which may have further accelerated flow velocity (see Section 5.1.1; Hallet, 1979; Herman et al., 2015; Patton et al., 2016). An increase in erosion rate towards the SB could thus be achieved through increased ice flux and velocity alone. In addition to that, Yanites et al. (2017) attributed generally lower erosional resistance (to fluvial downcutting) to the Wildegg Fm. when compared to the «Malmkalk» (see also (Pomper et al., 2017). This is supported not only by their slope-forming and cliff-forming nature (see Fig. 7), respectively, but also by our drill cores: in contrast to the «Malmkalk», the Wildegg Fm. is occasionally soft or disintegrating (see also Laws et al., 2007), and in the GST infill its clasts are not preserved, except for individual soft fragments in the lowermost ~0.4 m of QUST. Finally, additional structural weakening of the bedrock below the SB can again not be excluded (see e.g. Haldimann et al., 1984, and faults mapped by Matousek et al., 2000).

It should be noted that a potential narrow and steep-walled inner gorge (Dürst Stucki et al., 2010; Jansen et al., 2014; Montgomery and Korup, 2011) inside the GST could possibly not be imaged by our chosen methodology. This is due to the spacing of acquisition points, and due to the HVSR peak widening related to steeply inclined reflectors (Dietiker et al., 2018). The existence of such a gorge can thus not be excluded. Below the trough centre at line A (Fig. 5, Fig. B.1), the inconclusive log of a (destructively drilled) geothermal probe records unconsolidated sand to a depth slightly below 200 m a.s.l. With regard to our seismic measurements (which are in good accordance with Pietsch and Jordan, 2014), we interpret a singular gravel layer at 245 m a.s.l. as coarse-grained sediment at the base of the Gebenstorf-Stilli Trough, but a significantly deeper trough base is possible at this position.

The morphology of the GST is in strong contrast to the Birrfeld Basin, from which it originates, and which is significantly wider (>3.5 km at 300 m a.s.l.; Figs. 1, 2) and deeper (<150 m a.s.l.; Pietsch and Jordan, 2014). Aside from the differing dominant bedrock lithologies (Molasse vs. Mesozoic, respectively; Bitterli-Dreher et al., 2007; Jordan, 2010), this is likely a consequence of the position and multiphase origin of the Birrfeld. We suspect that the FJ had a damming effect on the Pleistocene ice advances into the foreland, with ice repeatedly accumulating, basal melt water flow concentrating, and subglacial erosion focusing just south of it (approx. at the local LGM; Bini et al., 2009). As a result, the Birrfeld Basin is composed of several inlaid basin generations (Graf, 2009; Jordan, 2010; Nitsche et al., 2001). The same effect could explain the widening of the terminal Seetal Valley overdeepening below the town of Rupperswil (Fig. 1; Pietsch and Jordan, 2014).

5.2.2. Mechanisms of overdeepening erosion

Our study reveals that the «Malmkalk» was relatively resistant to the subglacial erosion that excavated the trough (Fig. 6). We infer this predominantly from the morphology of the GST that shallows abruptly upon reaching the limestone, and deepens again immediately after the limestone is breached. Although the abundant stylolites and fault planes as well as karst features of the «Malmkalk» should have facilitated glacial erosion sensu stricto by quarrying (Dühnforth et al., 2010; Krabbendam and Glasser, 2011), this erosion process was apparently rather inefficient. Relatively low glacial erosion efficiency is further supported by the low percentage of locally derived limestone clasts in the basal coarse-grained trough infill: with exception of the lowermost few decimeters of QGBR and QUST, it is not significantly higher than in the Niederterrasse gravels at the top of the GST infill (Fig. 4). In addition, the bedrock directly below the base of the GST, even where it is pervaded by paleokarst (Gegg et al., 2020), is generally intact without evidence for glaciotectonic crushing or shearing at the former ice-bed interface (van der Wateren, 2002). Although the representativity of three boreholes is low, the absence of glaciotectonic structures indicates that ice-bed coupling, and therefore glacial erosivity, was limited at least during the final stage of the GST incision (Hart and Boulton, 1991; Lee and Phillips, 2013). This is a consequence of high basal water pressure at the glacier base (Piotrowski and Tulaczyk, 1999; Fischer and Clarke, 2001; Buechi et al., 2017), of which presumed hydrofractures within the paleokarst in QGBR provide additional record (Gegg et al., 2020).

These observations support the idea that subglacial water played a crucial role during the excavation of the GST. Periodically, basal water flow must have been sufficiently high to strip debris off the glacier bed and evacuate it out of the overdeepening, in order to enable ongoing erosion (Alley et al., 1997, 2019; Cook and Swift, 2012; Buechi et al., 2017). This flushing appears to have been rather efficient, because little basal coarse-grained sediment is preserved in the GST (<10 m in QGBR and QGVO; Fig. 4), and because large parts of this sediment are gravelly instead of diamictic, i.e. have been washed out or reworked. While the terminal (between lines G and H; ~1.6°) as well as the internal adverse slope of the GST (between lines B and E; ~1.9°) are comparatively steep (Table 1), they obviously did not significantly impede the evacuation of water and sediment from the basin (cf. Hooke, 1991; Alley et al., 1997; Cook and Swift, 2012). Consequently, much steeper adverse slope sections exist within Swiss foreland overdeepenings (e.g. in the Lower Glatt Valley; Buechi et al., 2017; see also Pietsch and Jordan, 2014).

Our findings can be interpreted in order to support the idea that subglacial water was in fact the main driver of erosion of the GST (Dürst Stucki et al., 2010; Fiore et al., 2011; Dürst Stucki and Schlunegger, 2013). This would explain the resilience of the «Malmkalk», as its decimeter- to meter-scale fracture spacing could be too large to allow for plucking by fluid water (Whipple et al., 2000; Sklar and Dietrich, 2001). In contrast, subglacial erosion of sand- and siltstone (Molasse) and marl (Wildegg Fm., Molasse) was far more efficient in the GST (Fig. 6; Ndiaye et al., 2014). Compared to the Villigen Fm. limestone, the rather poorly lithified Molasse, and likely also the locally soft or disintegrating Wildegg Fm., are more readily eroded grain-by-grain by flowing water. The build-up of elevated pore pressures above impermeable interbeds or above the lower-permeability «Malmkalk», and associated liquefaction (Janszen et al., 2012; Ravier et al., 2015; Wenau and Alves, 2020), may have further enhanced erosion in these softer lithologies.

Whether this presumed subglacial erosion by water occurs predominantly through the long-term steady flow of seasonal melt water (e.g. Mooers, 1989) or through catastrophic outburst of subglacial reservoirs ('jökulhlaups'; e.g. Shaw, 2002) is subject to debate (Alley et al., 2019). Both models are conceivable in the case of the GST: in the study area, three major regional drainage routeways (Aare, Reuss, Limmat) with a combined present-day catchment area of over 17′500 km^2 collide, capable of delivering vast amounts of meteoric and melt water. Additionally, it is conceivable that outburst events e.g. from the Birrfeld Basin could have released short-lived pulses of subglacial water (Fig. 2B; Gegg et al., 2020).

6. Summary and conclusions

With the aim of better constraining the morphology of the overdeepened Gebenstorf-Stilli Trough (GST), a seismic campaign employing surface wave analysis was conducted. The combined

approach of active and passive measurements succeeded at imaging the trough base and, calibrated and complemented with borehole data, allowed us to develop a well-constrained model of the GST (Fig. 7) that is currently being incorporated into an updated version of the Base of Quaternary model of Northern Switzerland by Nagra (Loepfe et al., 2021). The chosen methodology is therefore a well-suited and cost-effective approach for mapping overdeepened basins.

Our results suggest that the trough morphology is considerably controlled by the underlying bedrock geology. Due to relatively high erosional resistance, resulting high relief and constrained ice flow conditions, the overdeepening is inner-Alpine-like and narrow across the Folded Jura. In contrast, where it transitions into the weaker Molasse deposits further north, the GST becomes wider and more sinuous, similar to other foreland overdeepenings. The trough widening in the Molasse is interpreted as a consequence of less constrained ice flow but likely also of the underlying, more resistant «Malmkalk» (Jurassic limestone) rising towards the north. The trough shallowing culminates in a bedrock ridge whose top lies close to the lowest known Pleistocene base level (i.e. in non-overdeepened position). Further north, erosion depth increased again resulting in a second sub-basin. This is due to weaker marls underlying the trough, aided by ice flow being again topographically constrained and possibly increased due to glacier confluence. Thus, we propose that bedrock geology and ensuing topography exert substantial control on subglacial overdeepening erosion. In addition, we suspect that based on borehole data, the morphological complexity of overdeepenings may generally be underestimated.

The different resiliences to subglacial erosion together with a lack of evidence of glaciotectonism as well as the composition of the basal coarse-grained trough infill, which is poor in locally derived material, suggest that both glacial coupling and therefore glacial erosion sensu stricto, especially through plucking, was relatively inefficient in the GST. In contrast, the scarcity of well-preserved basal diamict, signs of subglacial hydrofracturing, as well as the paleoglaciological setting in general indicate that availability and pressure of basal water must have been periodically very high. This basal water played a significant role in overdeepening erosion, and we consider possible that it may have been its main driver. This would render the GST and other Alpine foreland overdeepenings analogs of tunnel valleys, as has previously been suggested.

However, it would probably be an oversimplification to attribute any given overdeepening to exclusively glacial or melt water erosion. The subglacial incision process is likely more complex, and the dominant mechanisms time-dependant (e.g. glacial erosion during peak glacial conditions, and enlargement by melt water during deglaciation). It should be noted that studies investigating erosion by melt water and its geological controls are restricted to the subaerial environment. The erosive impact of subglacial water on the overdeepened glacier bed is poorly understood, and should be targeted by future work.

Data availability

The data that support the findings of this study are available from the corresponding author upon reasonable request.

Declaration of competing interest

The authors declare that they have no known competing financial interests or personal relationships that could have appeared to influence the work reported in this paper.

Acknowledgements

This study was funded by the Swiss National Cooperative for the Disposal of Radioactive Waste (Nagra). Nagra designed the drilling and seismic campaign in close cooperation with the authors, who conducted data acquisition and interpretation in a joint effort. We would further like to thank Giancarlo Dal Moro (Eliosoft, analysis of MFA and ESAC data), Mirko Marsano, Dave Kündig, Claudia Keller (assistance during the seismic field campaign) as well as the cantonal authorities of Aargau for providing valuable borehole data. This manuscript benefited from the editorial handling by Markus Stoffel, and constructive reviews by Darrel Swift as well as a second anonymous reviewer.

Appendix A. Supplementary data

Supplementary data to this article can be found online at https://doi.org/10.1016/j.geomorph.2021.107950.

References

Alley, R., Cuffey, K., Evenson, E., Strasser, J., Lawson, D., Larson, G., 1997. How glaciers entrain and transport basal sediment: physical constraints. Quat. Sci. Rev. 16 (9), 1017–1038.
Alley, R., Cuffey, K., Zoet, L., 2019. Glacial erosion: status and outlook. Ann. Glaciol. 1–13.
Augustinus, P.C., 1992. The influence of rock mass strength on glacial valley cross-profile morphometry: a case study from the Southern Alps, New Zealand. Earth Surf. Process. Landf. 17 (1), 39–51.
Becker, R.A., Tikoff, B., Riley, P.R., Iverson, N.R., 2014. Preexisting fractures and the formation of an iconic American landscape: Tuolumne Meadows, Yosemite National Park, USA. GSA Today 24 (11), 4–10.
Berger, J.-P., Reichenbacher, B., Becker, D., Grimm, M., Grimm, K., Picot, L., Storni, A., Pirkenseer, C., Derer, C., Schaefer, A., 2005. Paleogeography of the upper Rhine Graben (URG) and the Swiss Molasse basin (SMB) from Eocene to Pliocene. Int. J. Earth Sci. 94 (4), 697–710.
Bini, A., Buoncristiani, J.F., Couterrand, S., Ellwanger, D., Felber, M., Florineth, D., Graf, H.R., Keller, O., Kelly, M., Schlüchter, C., 2009. Die Schweiz während des letzteiszeitlichen Maximums (LGM) 1:500.000. Bundesamt für Landestopographie swisstopo.
Bitterli-Dreher, P., Graf, H.R., Naef, H., Diebold, P., Matousek, F., Burger, H., Pauli-Gabi, T., 2007. Geologischer Atlas der Schweiz 1:25.000. Blatt 1070 Baden. Erläuterungen. Bundesamt für Landestopografie swisstopo, Wabern, Switzerland.
Brook, M.S., Kirkbride, M.P., Brock, B.W., 2004. Rock strength and development of glacial valley morphology in the Scottish Highlands and northwest Iceland. Geogr. Annal. Ser. A Phys. Geogr. 86 (3), 225–234.
Buechi, M.W., Frank, S.M., Graf, H.R., Menzies, J., Anselmetti, F.S., 2017. Subglacial emplacement of tills and meltwater deposits at the base of overdeepened bedrock troughs. Sedimentology 64 (3), 658–685.
Burkhard, M., 1990. Aspects of the large-scale Miocene deformation in the most external part of the Swiss Alps (sub-Alpine molasse to Jura fold belt). Eclogae Geol. Helv. 83 (3), 559–583.
Cofaigh, C.O., 1996. Tunnel valley genesis. Progress in physical geography 20 (1), 1–19.
Cohen, D., Hooyer, T.S., Iverson, N.R., Thomason, J., Jackson, M., 2006. Role of transient water pressure in quarrying: a subglacial experiment using acoustic emissions. J. Geophys. Res. Earth Surf. 111, F03006.
Commission for the Geological Map of the World, Asch, K., Bellenberg, S., 2005. The 1:5 Million International Geological Map of Europe and Adjacent Areas (IGME 5000). Bundesanstalt für Geowissenschaften und Rohstoffe.
Cook, S.J., Swift, D.A., 2012. Subglacial basins: their origin and importance in glacial systems and landscapes. Earth Sci. Rev. 115 (4), 332–372.
Dal Moro, G., Moustafa, S.S., Al-Arifi, N.S., 2018. Improved holistic analysis of Rayleigh waves for single- and multi-offset data: joint inversion of Rayleigh-wave particle motion and vertical-and radial-component velocity spectra. Pure Appl. Geophys. 175 (1), 67–88.
Deplazes, G., Bläsi, H., Schnellmann, M., Traber, D., 2013. Sedimentologie und Stratigraphie der Effinger Schichten. Nagra Arbeitsbericht NAB, pp. 13–16.
Diebold, P., Bitterli-Brunner, P., Naef, H., 2006. Geologischer Atlas der Schweis 1:25′000, Blatt 1069/1049 Frick-Laufenburg. Bundesamt für Landestopographie swisstopo, Wabern.
Dietiker, B., Pugin, A.J.-M., Crow, H.L., Mallozzi, S., Brewer, K.D., Cartwright, T.J., Hunter, J.A., 2018. HVSR measurements in complex sedimentary environment and highly structured resonator topography–comparisons with seismic reflection profiles and geophysical borehole logs. Symposium on the Application of Geophysics to Engineering and Environmental Problems. 2018, pp. 324–330.
Dühnforth, M., Anderson, R.S., Ward, D., Stock, G.M., 2010. Bedrock fracture control of glacial erosion processes and rates. Geology 38 (5), 423–426.
Dürst Stucki, M., Schlunegger, F., 2013. Identification of erosional mechanisms during past glaciations based on a bedrock surface model of the central European Alps. Earth Planet. Sci. Lett. 384, 57–70.
Dürst Stucki, M., Reber, R., Schlunegger, F., 2010. Subglacial tunnel valleys in the Alpine foreland: an example from Bern, Switzerland. Swiss J. Geosci. 103 (3), 363–374.
Dziewonski, A., Bloch, S., Landisman, M., 1969. A technique for the analysis of transient seismic signals. Bull. Seismol. Soc. Am. 59 (1), 427–444.
Fiore, J., Girardclos, S., Pugin, A., Gorin, G., Wildi, W., 2011. Würmian deglaciation of western Lake Geneva (Switzerland) based on seismic stratigraphy. Quat. Sci. Rev. 30 (3–4), 377–393.

Fischer, U.H., Clarke, G.K., 2001. Review of subglacial hydro-mechanical coupling: Trapridge glacier, Yukon Territory, Canada. Quat. Int. 86 (1), 29–43.
Gegg, L., Kuster, A.M., Amschwand, D., Huber, M., Deplazes, G., Madritsch, H., Buechi, M.W., 2019a. Quaternary Borehole QBO Gebenstorf-Vogelsang (QGVO) Data Report. Nagra Arbeitsbericht NAB 19-03.
Gegg, L., Kuster, A.M., Deplazes, G., Madritsch, H., Buechi, M.W., 2019b. Quaternary Borehole QBO Gebenstorf-Brüel (QGBR) Data Report. Nagra Arbeitsbericht NAB 19-02.
Gegg, L., Kuster, A.M., Schmid, D., Lemke, K., Deplazes, G., Madritsch, H., Buechi, M.W., 2019c. Quaternary Borehole QBO Untersiggenthal (QUST) Data Report. Nagra Arbeitsbericht NAB 19-01.
Gegg, L., Buechi, M.W., Ebert, A., Deplazes, G., Madritsch, H., Anselmetti, F.S., 2020. Brecciation of glacially overridden palaeokarst (Lower Aare Valley, northern Switzerland): result of subglacial water-pressure peaks? Boreas 49 (4), 813–827.
Glasser, N.F., Crawford, K.R., Hambrey, M.J., Bennett, M.R., Huddart, D., 1998. Lithological and structural controls on the surface wear characteristics of glaciated metamorphic bedrock surfaces: Ossian Sarsfjellet, Svalbard. J. Geol. 106 (3), 319–330.
Goudie, A.S., 2016. Quantification of rock control in geomorphology. Earth Sci. Rev. 159, 374–387.
Graf, H.R., 2009. Stratigraphie von Mittel-und Spätpleistozän in der Nordschweiz. Beiträge zur Geologischen Karte der Schweiz. Bundesamt für Landestopografie swisstopo, Wabern, Switzerland.
Graf, H.R., Bitterli-Dreher, P., Burger, H., Bitterli, T., Diebold, P., Naef, H., 2006. Geologischer Atlas der Schweiz 1:25′000, Blatt 1070 Baden. Bundesamt für Landestopografie swisstopo, Wabern, Switzerland.
Gygi, R.A., 2000. Integrated Stratigraphy of the Oxfordian and Kimmeridgian (Late Jurassic) in Northern Switzerland and Adjacent Southern Germany. Birkhäuser, Basel.
Haldimann, P., Naef, H., Schmassmann, H., 1984. Fluviatile Erosions-und Akkumulationsformen als Indizien jungpleistozäner und holozäner Bewegungen in der Nordschweiz und angrenzenden Gebieten. Nagra Technischer Bericht NTB 84 (16).
Hallet, B., 1979. A theoretical model of glacial abrasion. J. Glaciol. 23 (89), 39–50.
Harbor, J.M., 1995. Development of glacial-valley cross sections under conditions of spatially variable resistance to erosion. Geomorphology 14 (2), 99–107.
Hart, J.K., Boulton, G.S., 1991. The interrelation of glaciotectonic and glaciodepositional processes within the glacial environment. Quat. Sci. Rev. 10 (4), 335–350.
Herman, F., Beaud, F., Champagnac, J.-D., Lemieux, J.-M., Sternai, P., 2011. Glacial hydrology and erosion patterns: a mechanism for carving glacial valleys. Earth Planet. Sci. Lett. 310 (3), 498–508.
Herman, F., Beyssac, O., Brughelli, M., Lane, S.N., Leprince, S., Adatte, T., Lin, J.Y., Avouac, J.-P., Cox, S.C., 2015. Erosion by an Alpine glacier. Science 350 (6257), 193–195.
Hooke, R.L., 1991. Positive feedbacks associated with erosion of glacial cirques and overdeepenings. Geol. Soc. Am. Bull. 103 (8), 1104–1108.
Hooyer, T.S., Cohen, D., Iverson, N.R., 2012. Control of glacial quarrying by bedrock joints. Geomorphology 153, 91–101.
Jansen, J.D., Codilean, A.T., Stroeven, A.P., Fabel, D., Hättestrand, C., Kleman, J., Harbor, J.M., Heyman, J., Kubik, P.W., Xu, S., 2014. Inner gorges cut by subglacial meltwater during Fennoscandian ice sheet decay. Nat. Commun. 5 (1), 1–7.
Janszen, A., Spaak, M., Moscariello, A., 2012. Effects of the substratum on the formation of glacial tunnel valleys: an example from the Middle Pleistocene of the southern North Sea Basin. Boreas 41 (4), 629–643.
Jordan, P., 2010. Analysis of overdeepened valleys using the digital elevation model of the bedrock surface of Northern Switzerland. Swiss J. Geosci. 103 (3), 375–384.
Jordan, P., Wetzel, A., Reisdorf, A., 2008. Swiss Jura Mountains. Pienkowski, G., & Schudack, M. (coordinators). Jurassic. In: McCann, T. (Ed.), The Geology of Central Europe, Second ed., pp. 823–923.
Jordan, P., Eberhard, M., Graf, H.R., Diebold, P., Jost, J., Schurch, R., 2011. Geologischer Atlas der Schweiz 1:25′000, Blatt 1089 Aarau. Bundesamt für Landestopografie swisstopo, Wabern.
Jordan, P., Malz, A., Heuberger, S., Pietsch, J., Kley, J., Madritsch, H., 2015. Regionale geologische Profilschnitte durch die Nordschweiz und 2D-Bilanzierung der Fernschubdeformation im östlichen Faltenjura: Arbeitsbericht zu SGT Etappe 2. Nagra Arbeitsbericht NAB, pp. 14–105.
Keller, O., Krayss, E., 2010. Mittel-und spätpleistozäne Stratigraphie und Morphogenese in Schlüsselregionen der Nordschweiz. E&G: Quat. Sci. J. 59 (1–2), 88–119.
Krabbendam, M., Glasser, N.F., 2011. Glacial erosion and bedrock properties in NW Scotland: abrasion and plucking, hardness and joint spacing. Geomorphology 130 (3–4), 374–383.
Kühni, A., Pfiffner, O.-A., 2001. The relief of the Swiss Alps and adjacent areas and its relation to lithology and structure: topographic analysis from a 250-m DEM. Geomorphology 41 (4), 285–307.
Laubscher, H.P., 1962. Die Zweiphasenhypothese der Jurafaltung. Eclogae Geol. Helv. 55, 1–22.
Laws, S., Deplazes, G., Jäckli, H., 2007. Geologie und Hydrogeologie der Effinger Schichten im Tafeljura und am Jurasüdfuss. Nagra Arbeitsbericht NAB 07-28.
Lee, J.R., Phillips, E., 2013. Glacitectonics—a key approach to examining ice dynamics, substrate rheology and ice-bed coupling. Proc. Geol. Assoc. 124 (5), 731–737.
Loepfe, R., et al., 2021. Digitales Höhenmodell Basis Quartär der Nordschweiz – Version 2021 und ausgewählte Auswertungen. Nagra Arbeitsbericht (in prep.).
Looser, N., Madritsch, H., Guillong, M., Laurent, O., Wohlwend, S., Bernasconi, S., 2021. Absolute age and temperature constraints on deformation along the basal décollement of the Jura fold-and-thrust belt from carbonate U-Pb dating and clumped isotopes. Tectonics 40 (3), e2020TC006439.
MacGregor, K., Anderson, R., Anderson, S., Waddington, E., 2000. Numerical simulations of glacial-valley longitudinal profile evolution. Geology 28 (11), 1031–1034.
Madritsch, H., 2015. Outcrop-scale fracture systems in the Alpine foreland of central northern Switzerland: kinematics and tectonic context. Swiss J. Geosci. 108 (2–3), 155–181.
Madritsch, H., Meier, B., Kuhn, P., Roth, P., Zingg, O., Heuberger, S., Naef, H., Birkhäuser, P., 2013. Regionale strukturgeologische Zeitinterpretation der Nagra 2D-Seismik 2011/12. Nagra Arbeitsbericht NAB 13-10.
Magrani, F., Valla, P., Gribenski, N., Serra, E., 2020. Glacial overdeepenings in the Swiss Alps and foreland: spatial distribution and morphometrics. Quat. Sci. Rev. 243, 106483.
Malz, A., Madritsch, H., Kley, J., 2015. Improving 2D seismic interpretation in challenging settings by integration of restoration techniques: a case study from the Jura fold-and-thrust belt (Switzerland). Interpretation 3 (4), SAA37–SAA58.
Matousek, F., Wanner, M., Baumann, A., Graf, H., Nüesch, R., Bitterli, T., 2000. Geologischer Atlas der Schweiz 1:25′000. Blatt 102 Zurzach. Wabern, Switzerland, Bundesamt für Landestopografie swisstopo.
Montgomery, D.R., Korup, O., 2011. Preservation of inner gorges through repeated Alpine glaciations. Nat. Geosci. 4 (1), 62–67.
Mooers, H.D., 1989. On the formation of the tunnel valleys of the Superior lobe, central Minnesota. Quat. Res. 32 (1), 24–35.
Nagra, 2019. Preliminary Horizon and Structure Mapping of the Nagra 3D Seismics JO-15 (Jura Ost) in Time Domain. Nagra Arbeitsbericht NAB 18-34.
Nagra, 2021. Morphology of the Overdeepened Gebenstorf-Stilli Trough (Lower Aare Valley) from Seismic Surface Wave Investigations. Nagra Arbeitsbericht NAB 21-18.
Nakamura, Y., 1989. A method for dynamic characteristics estimation of subsurface using microtremor on the ground surface. Railw. Techn. Res. Inst. Quart. Rep. 30 (1), 25–33.
Ndiaye, M., Clerc, N., Gorin, G., Girardclos, S., Fiore, J., 2014. Lake Neuchâtel (Switzerland) seismic stratigraphic record points to the simultaneous Würmian deglaciation of the Rhône Glacier and Jura Ice Cap. Quat. Sci. Rev. 85, 1–19.
Nitsche, F., Monin, G., Marillier, F., Graf, H., Ansorge, J., 2001. Reflection seismic study of Cenozoic sediments in an overdeepened valley of northern Switzerland: the Birrfeld area. Eclogae Geol. Helv. 94 (3), 363–371.
Ohori, M., Nobata, A., Wakamatsu, K., 2002. A comparison of ESAC and FK methods of estimating phase velocity using arbitrarily shaped microtremor arrays. Bull. Seismol. Soc. Am. 92 (6), 2323–2332.
Patton, H., Swift, D., Clark, C., Livingstone, S.J., Cook, S.J., 2016. Distribution and characteristics of overdeepenings beneath the Greenland and Antarctic ice sheets: implications for overdeepening origin and evolution. Quat. Sci. Rev. 148, 128–145.
Pfiffner, O.A., 1986. Evolution of the north Alpine foreland basin in the Central Alps. Spec. Publ. Int. Assoc. Sediment. 8, 219–228.
Phillips, E., Everest, J., Díaz-Doce, D., 2010. Bedrock controls on subglacial landform distribution and geomorphological processes: Evidence from the Late Devensian Irish Sea Ice Stream. Sediment. Geol. 232 (3–4), 98–118.
Pietsch, J., Jordan, P., 2014. Digitales Höhenmodell Basis Quartär der Nordschweiz - Version 2014 und ausgewählte Auswertungen. Nagra Arbeitsbericht NAB 14-02.
Piotrowski, J.A., Tulaczyk, S., 1999. Subglacial conditions under the last ice sheet in northwest Germany: ice-bed separation and enhanced basal sliding? Quat. Sci. Rev. 18 (6), 737–751.
Preusser, F., Reitner, J.M., Schlüchter, C., 2010. Distribution, geometry, age and origin of overdeepened valleys and basins in the Alps and their foreland. Swiss J. Geosci. 103 (3), 407–426.
Pomper, J., Salcher, B.C., Eichkitz, C., Prasicek, G., Lang, A., Lindner, M., Götz, J., 2017. The glacially overdeepened trough of the Salzach Valley, Austria: Bedrock geometry and sedimentary fill of a major Alpine subglacial basin. Geomorphology 295, 147–158.
Preusser, F., Graf, H.R., Keller, O., Krayss, E., Schlüchter, C., 2011. Quaternary glaciation history of northern Switzerland. E&G Quat. Sci. J. 60, 282–305.
Ravier, E., Buoncristiani, J.-F., Menzies, J., Guiraud, M., Clerc, S., Portier, E., 2015. Does porewater or meltwater control tunnel valley genesis? Case studies from the Hirnantian of Morocco. Palaeogeogr. Palaeoclimatol. Palaeoecol. 418, 359–376.
SESAME European Research Project, 2004. Guidelines for the Implementation of the H/V Spectral Ratio Technique on Ambient Vibrations Measurements, Processing and Interpretation. Commission, European.
Shaw, J., 2002. The meltwater hypothesis for subglacial bedforms. Quat. Int. 90 (1), 5–22.
Sklar, L.S., Dietrich, W.E., 2001. Sediment and rock strength controls on river incision into bedrock. Geology 29 (12), 1087–1090.
Sprecher, C., Müller, W., 1986. Geophysikalisches Untersuchungsprogramm Nordschweiz: Reflexionsseismik 82. Nagra Technischer Bericht NTB 84-15.
Stumm, D., 2010. Deep Glacial Erosion. Review With Focus on Tunnel Valleys in Northern Europe. Nagra Arbeitsbericht NAB 10-33.
Swisstopo, 2013. swissALTI3D. Federal Office of Topography swisstopo Wabern, Switzerland.
Terzaghi, R.D., 1965. Sources of error in joint surveys. Geotechnique 15 (3), 287–304.
van der Vegt, P., Janszen, A., Moscariello, A., 2012. Tunnel valleys: current knowledge and future perspectives. Geol. Soc. Lond. Spec. Publ. 368 (1), 75–97.
van der Wateren, D.M., 2002. Processes of glaciotectonism. Modern and Past Glacial Environments. Elsevier, pp. 417–443.
Wenau, S., Alves, T.M., 2020. Salt-induced crestal faults control the formation of Quaternary tunnel valleys in the southern North Sea. Boreas 49 (4), 799–812.
Whipple, K.X., Hancock, G.S., Anderson, R.S., 2000. River incision into bedrock: mechanics and relative efficacy of plucking, abrasion, and cavitation. Geol. Soc. Am. Bull. 112 (3), 490–503.
Wiemer, S., Danciu, L., Edwards, B., Marti, M., Fäh, D., Hiemer, S., Wössner, J., Cauzzi, C., Kästli, P., Kremer, K., 2016. Seismic Hazard Model 2015 for Switzerland (SUIhaz2015). Swiss Seismological Service, ETH, Zurich, Switzerland.
Yanites, B.J., Becker, J.K., Madritsch, H., Schnellmann, M., Ehlers, T.A., 2017. Lithologic effects on landscape response to base level changes: a modeling study in the context

of the Eastern Jura Mountains, Switzerland. J. Geophys. Res. Earth Surf. 122 (11), 2196–2222.

Ziegler, P.A., Fraefel, M., 2009. Response of drainage systems to Neogene evolution of the Jura fold-thrust belt and Upper Rhine Graben. Swiss J. Geosci. 102 (1), 57–75.

Zimmer, P.D., Gabet, E.J., 2018. Assessing glacial modification of bedrock valleys using a novel approach. Geomorphology 318, 336–347.

Zoet, L., Alley, R.B., Anandakrishnan, S., Christianson, K., 2013. Accelerated subglacial erosion in response to stick-slip motion. Geology 41 (2), 159–162.

3D morphology of a glacially overdeepened trough controlled by underlying bedrock geology

Lukas Gegg, Gaudenz Deplazes, Lorenz Keller, Herfried Madritsch, Thomas Spillmann, Flavio S. Anselmetti, & Marius W. Buechi

Supplementary material

Supp. A: Summary scheme of the pre-Quaternary stratigraphy of the study area (Fig. A.1).

Supp. B: Cross sections A to H, input data and interpretations (Fig. B.1-B.8).

Differences between seismic and drilled trough depth (Table B.1).

Supp. C: Sinuosities of distal foreland overdeepenings of Switzerland (Fig. C.1).

Supp. D: Structural survey of a major strike-slip fault in a «Malmkalk» outcrop (Fig. D.1).

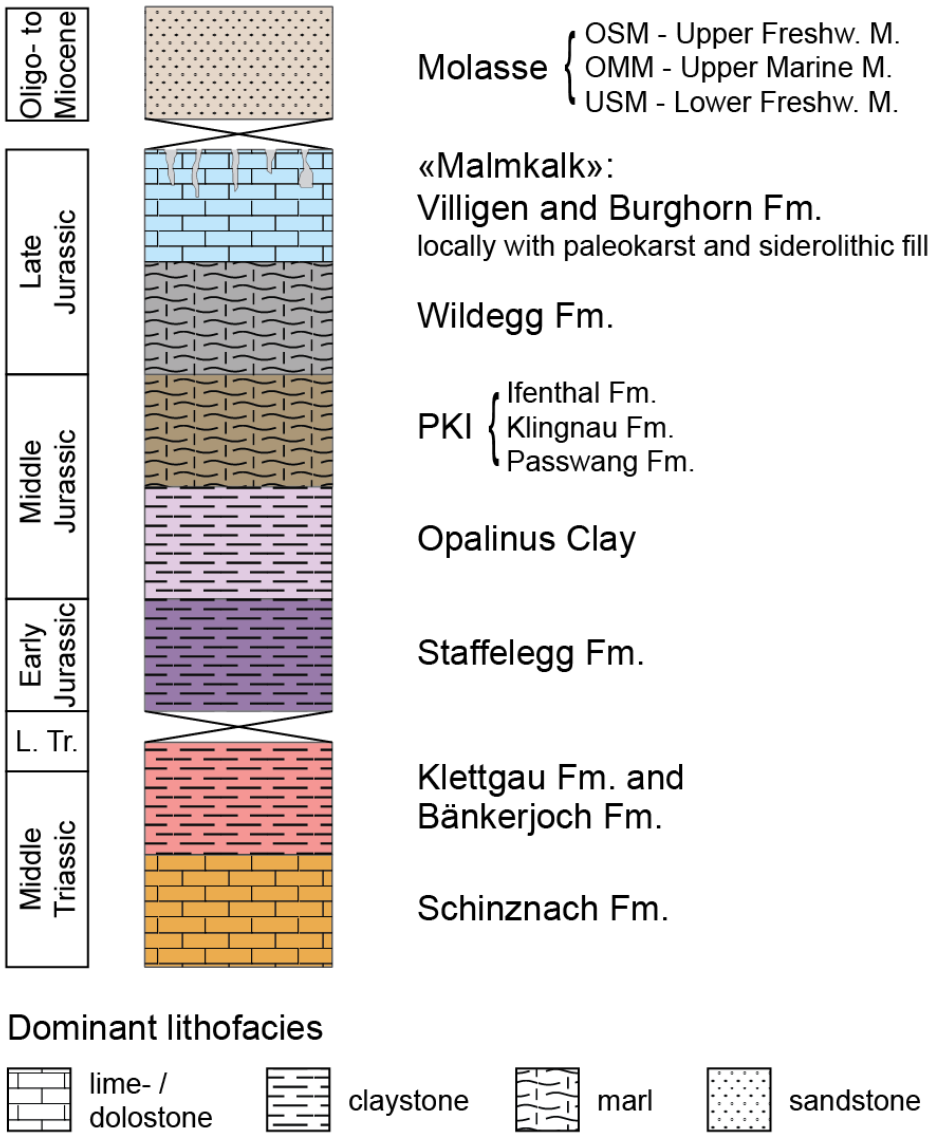

Fig. A.1: Summary scheme of the pre-Quaternary stratigraphy of the study area.

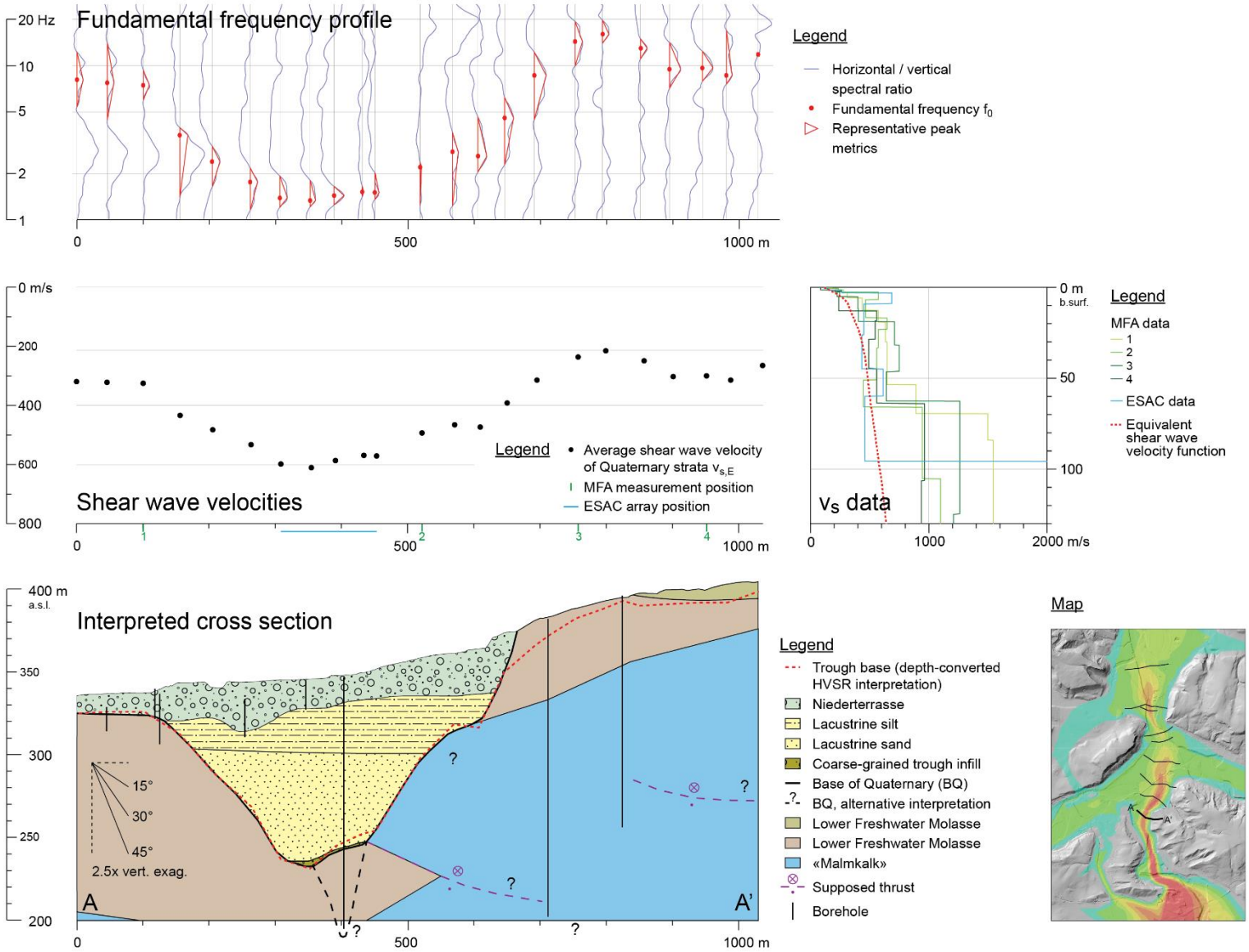

Fig. B.1: Cross section A, input data and interpretation.

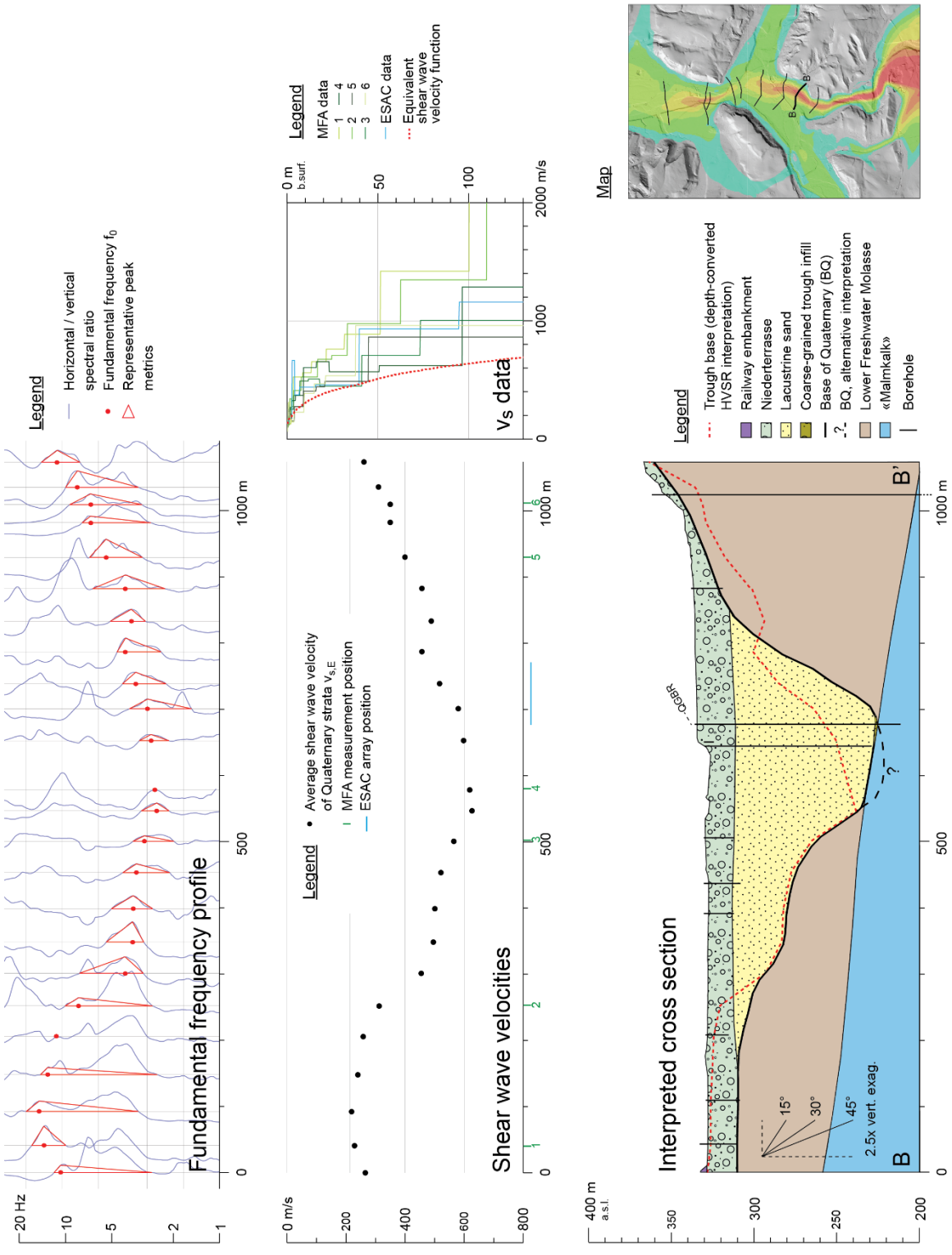

Fig. B.2: Cross section B, input data and interpretation.

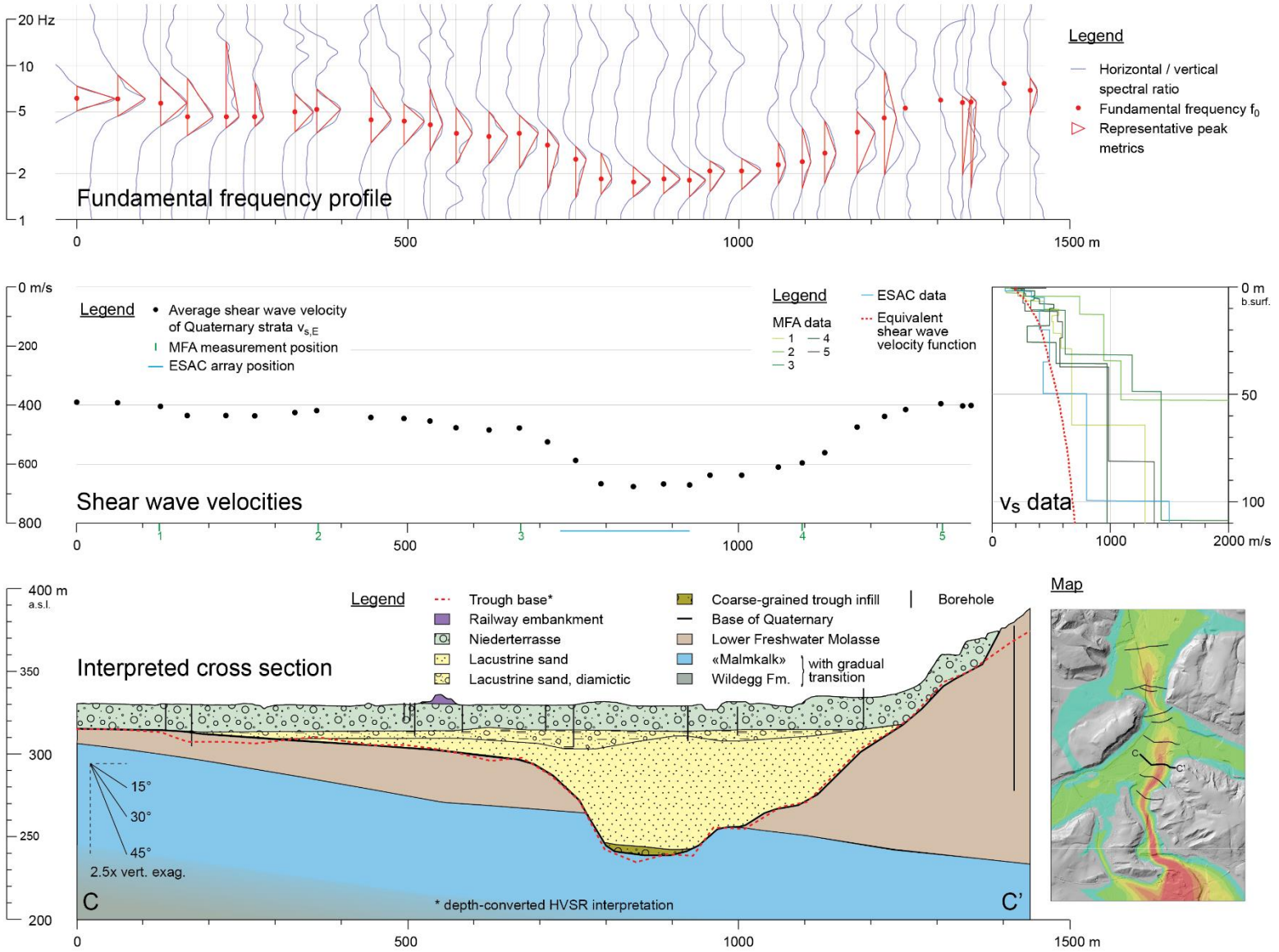

Fig. B.3: Cross section C, input data and interpretation.

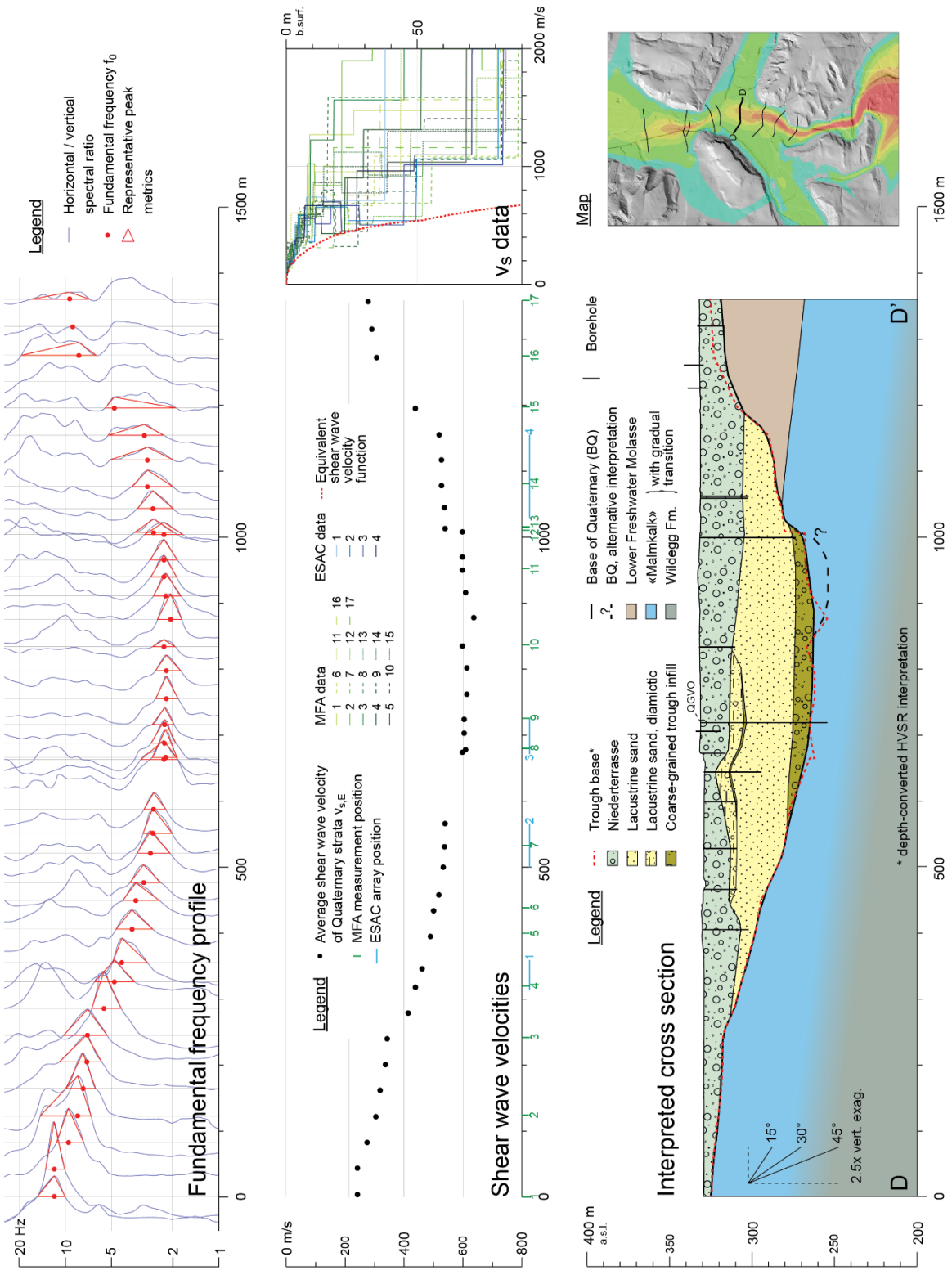

Fig. B.4: Cross section D, input data and interpretation.

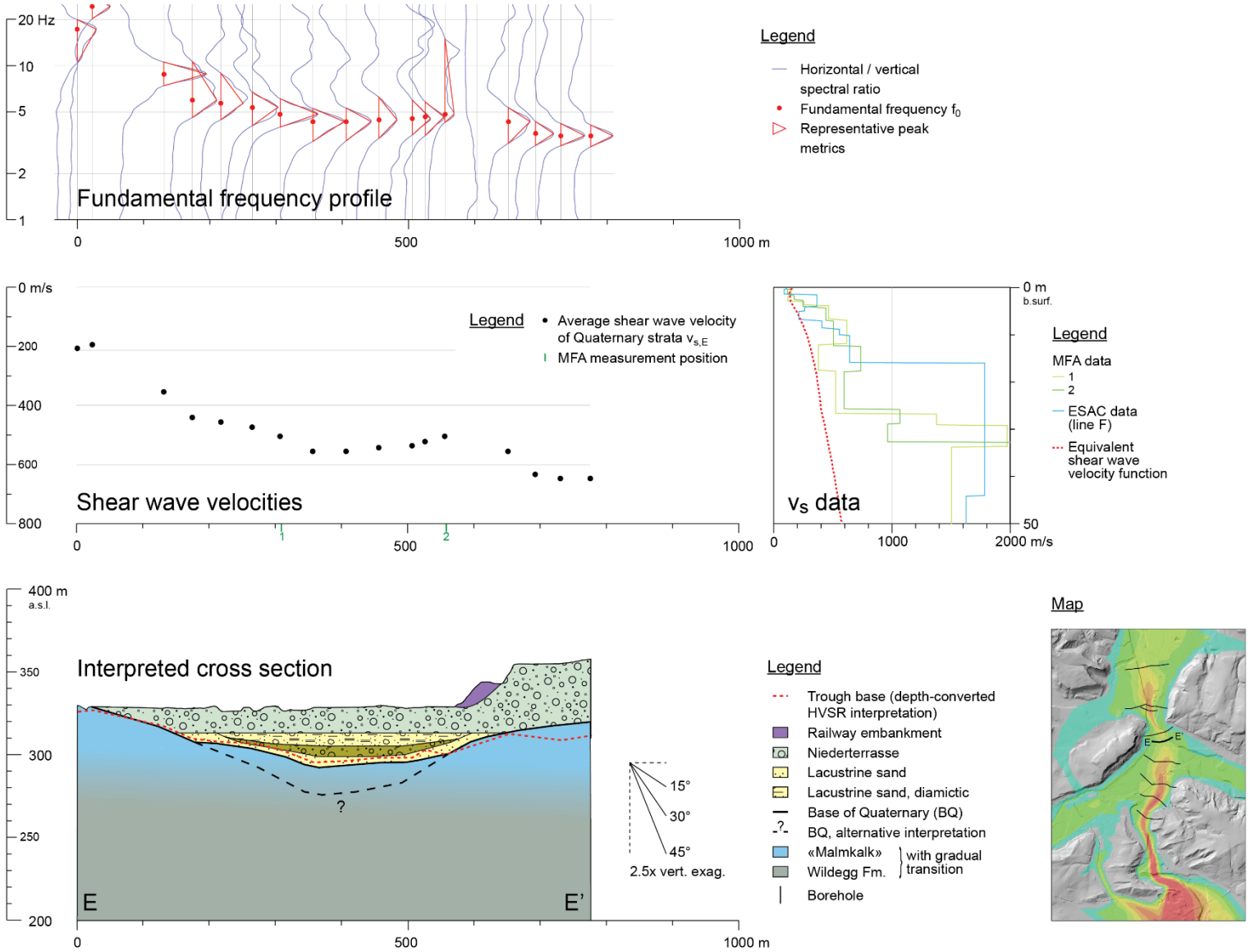

Fig. B.5: Cross section E, input data and interpretation.

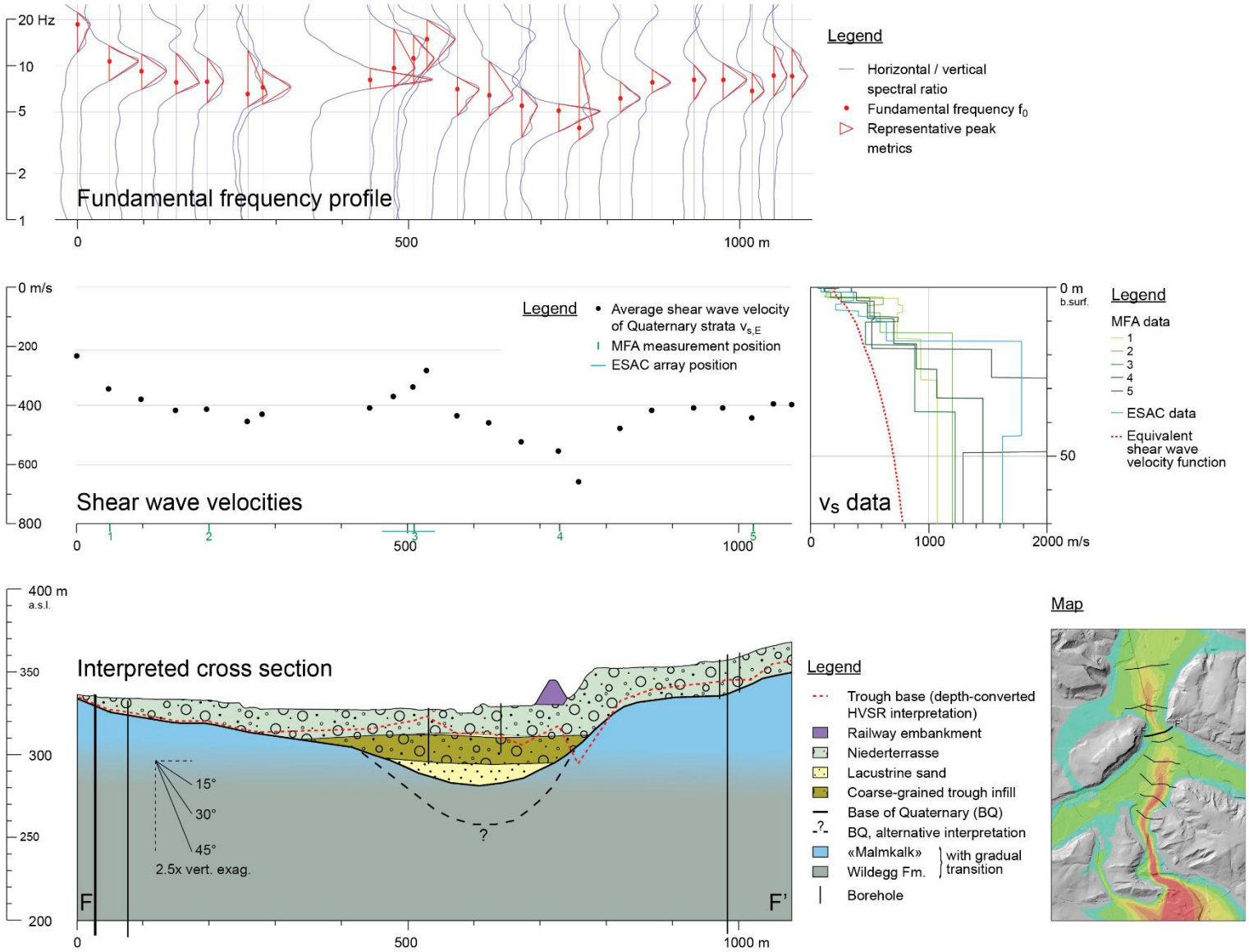

Fig. B.6: Cross section F, input data and interpretation.

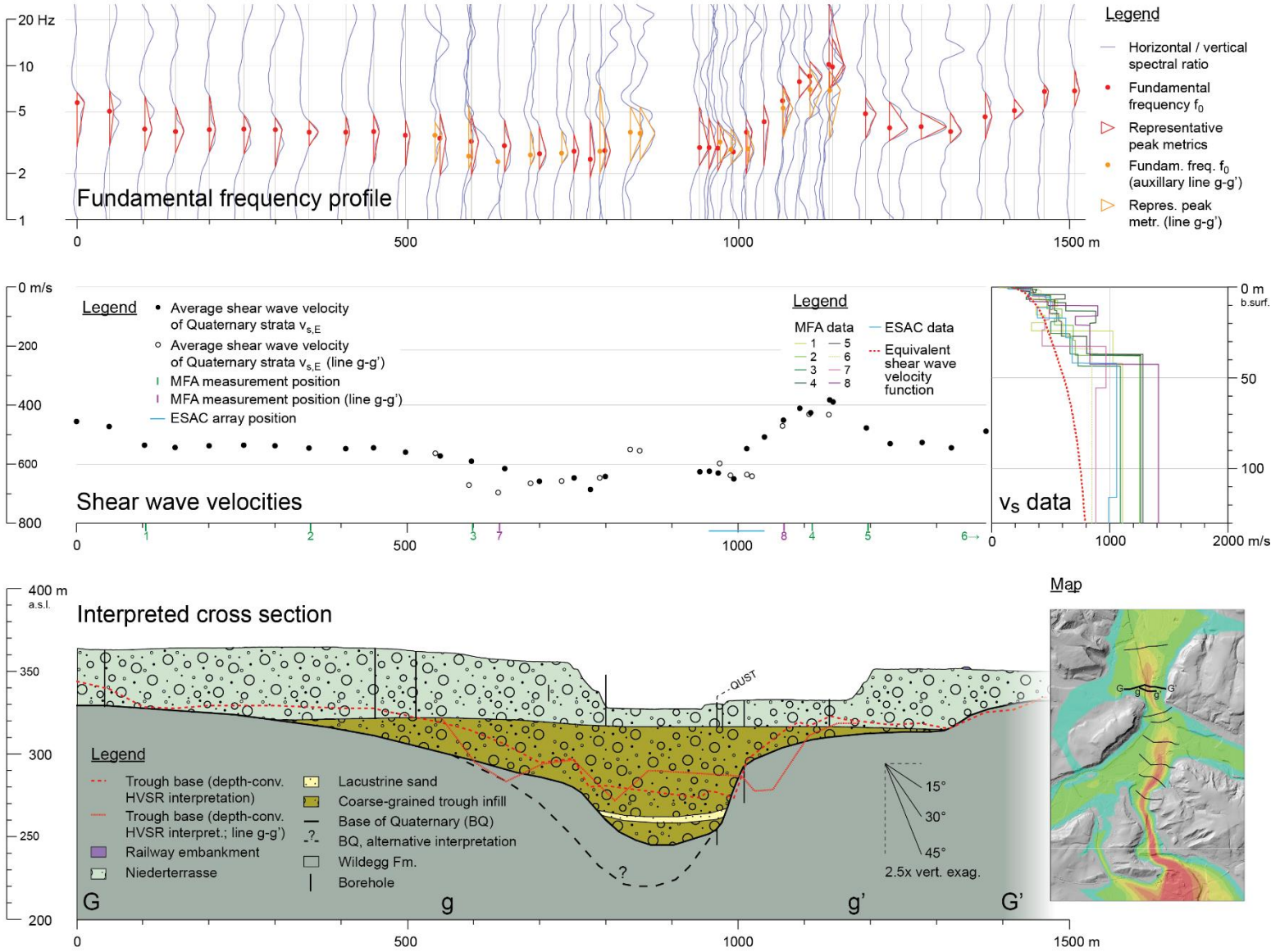

Fig. B.7: Cross section G, input data and interpretation.

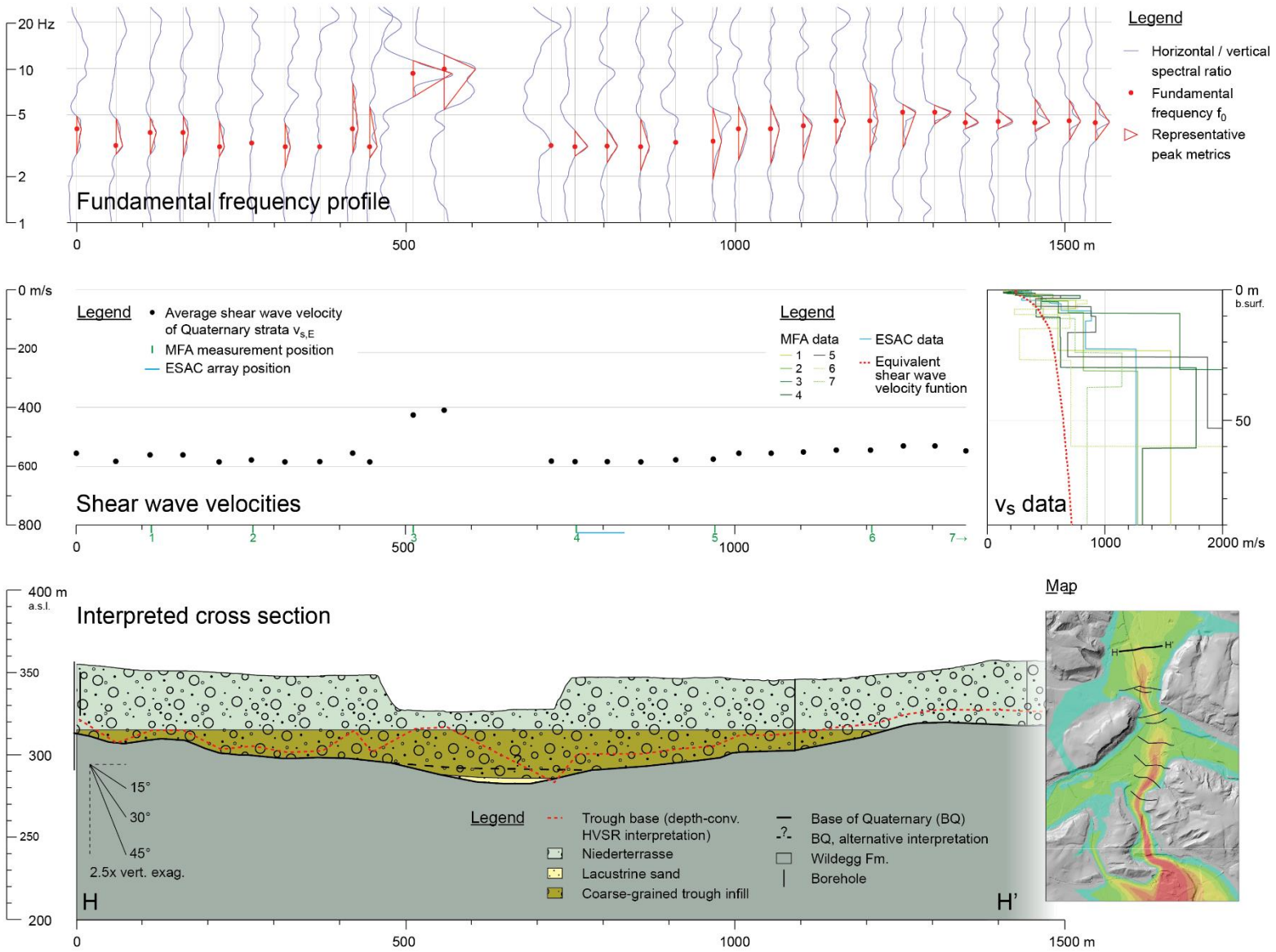

Fig. B.8: Cross section H, input data and interpretation.

Table B.1: Differences between seismic and drilled base of Quaternary (BQu) along the Gebenstorf-Stilli Trough based on drill logs from the borehole database of Nagra. Drilled values are marked with (?) if they are taken from logs that do not specifically identify the underlying bedrock, but the described lithology suggests its interpretation.

Sect.	Type	Distance [m]	BQu [m a.s.l.]		Difference [m]
			seismic	borehole	
A	Exploration borehole	170	325.9	316.0	9.9
A	Geothermal probe	0	322.3	322.8	-0.5
A	Geothermal probe	65	246.0	244.0 (?)	2.0
A	Geothermal probe	0	373.3	377.0	-3.7
A	Geothermal probe	0	393.3	377.0	16.3
B	Exploration borehole	20	392.5	398.0	-5.5
B	Geothermal probe	35	326.3	313.2	13.1
B	Exploration borehole	0	326.5	311.8	14.7
B	Exploration borehole	55	324.7	316.4	8.3
B	Scientific borehole QGBR	0	257.4	225.8	31.6
B	Exploration borehole	90	301.9	323.5	-21.6
B	Geothermal probe	55	335.1	349.0	-13.9
C	Exploration borehole	40	311.3	315.2	-3.9
C	Exploration borehole	85	307.1	312.7 (?)	-5.6
C	Geothermal probe	20	369.1	362.0	7.1
D	Scientific borehole QGVO	30	264.1	266.1	-2.0
D	Exploration borehole	0	324.0	317.7	6.3
E	Exploration borehole	50	311.9	319.9	-8.0
F	Geothermal probe	30	332.1	331.0	1.1
F	Geothermal probe	70	331.2	326.0	5.2
F	Geothermal probe	90	327.0	314.0	13.0
F	Exploration borehole	30	345.4	338.6	6.8
F	Geothermal probe	70	344.7	336.0	8.7
F	Exploration borehole	25	345.4	342.5	2.9
G	Exploration borehole	35	341.0	330.1	10.9
G	Exploration borehole	160	326.6	310.7 (?)	15.9
G	Exploration borehole	25	323.2	305.1 (?)	18.1
G	Scientific borehole QUST	0	276.0	255.2	20.8
G	Scientific boreh. (seismic survey)	155	296.4	291.0	3.4
G	Exploration borehole	140	321.6	312.2	9.4
H	Scientific boreh. (seismic survey)	25	321.0	315.3	5.7
H	Exploration borehole	175	320.4	324.0 (?)	3.6
H	Exploration borehole	0	326.6	318.2 (?)	8.4
				average	-7.2 / +9.8

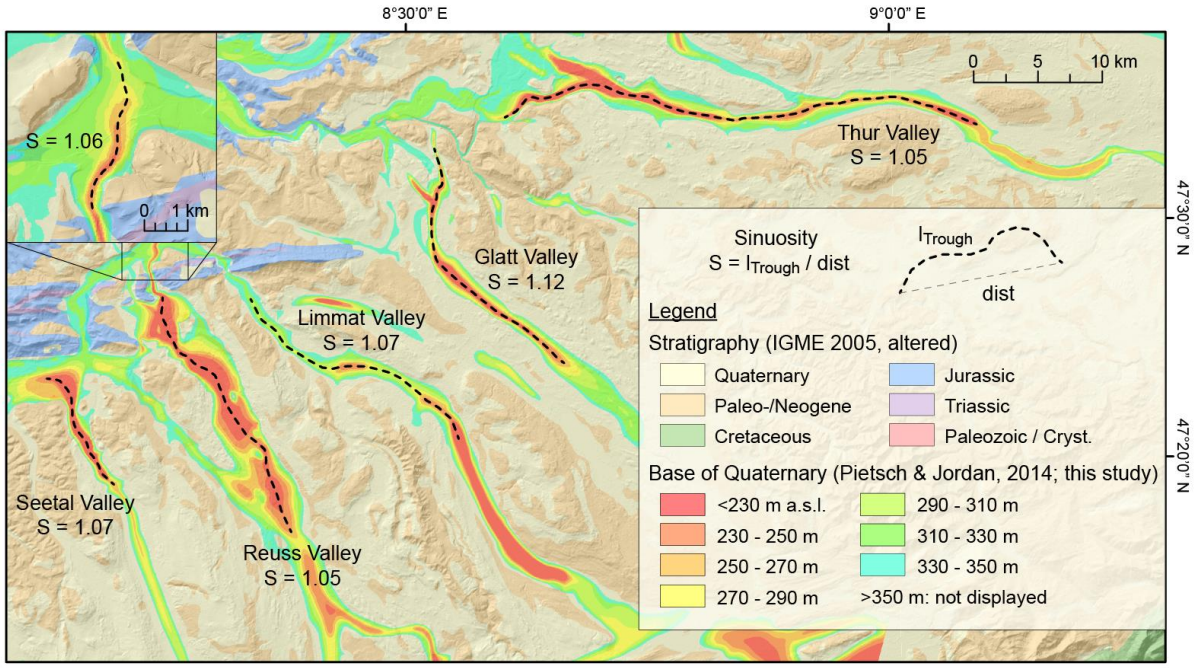

Fig. C.1: Sinuosities of major distal foreland overdeepenings of Switzerland. Note that the sinuosity of the central GST segment (zoom-in; S = 1.06) is similar to other Molasse-hosted overdeepenings.

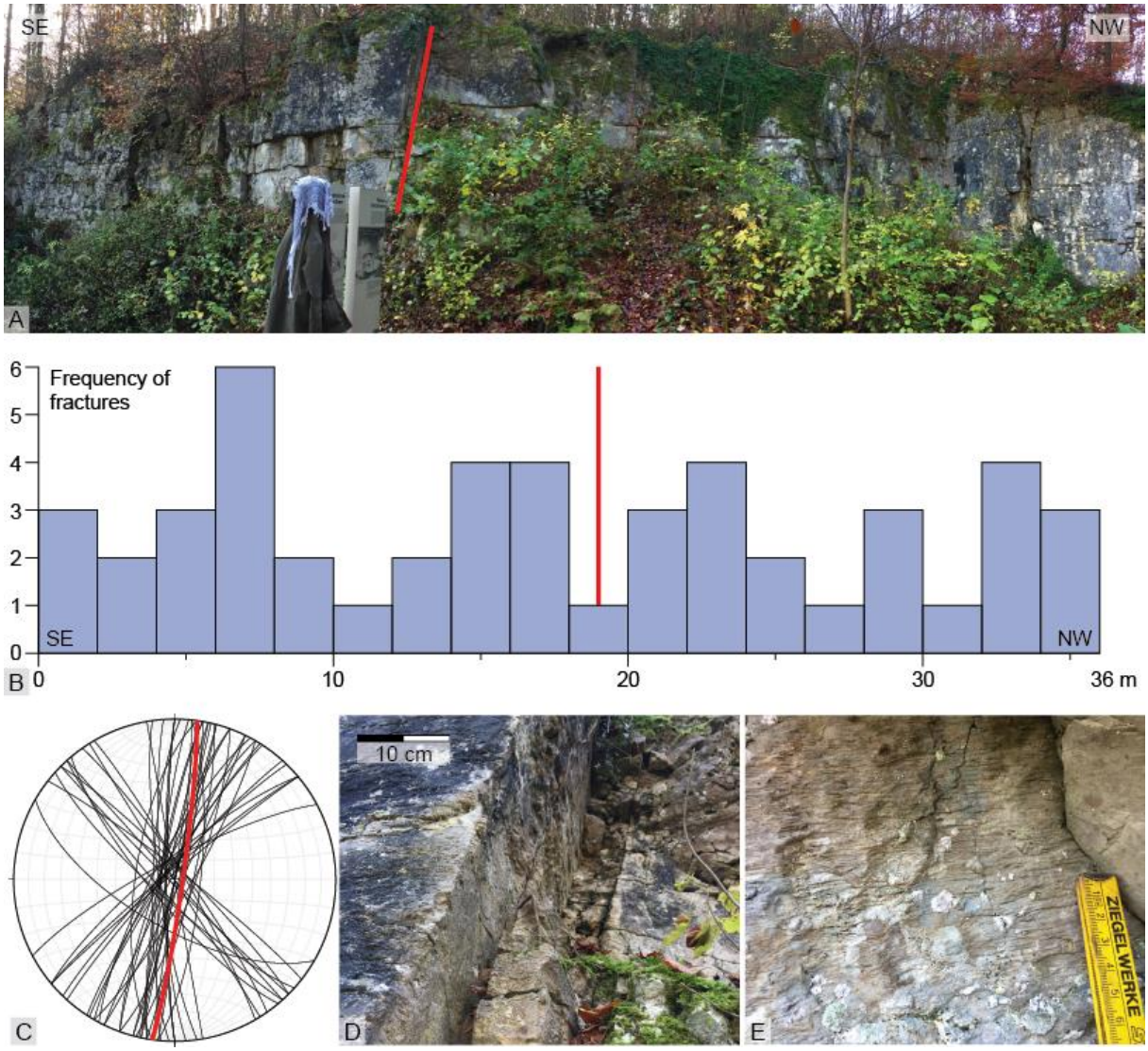

Fig. D.1: Structural survey of a «Malmkalk» outcrop (notheastern slope of Scherzberg; 47°26′43″ N, 8°10′40″ E) exposing a major strike-slip fault (red line on D.1A; panoramic photograph not to scale with D.1B). We observe no increased frequency of (striated) fractures in vicinity of the fault at 19 m along the outcrop wall (D.1B). Two groups of fractures occur, one with orientations similar to the major fault (10/85E, red line), one with a strike of ~140 (D.1C). D.1D: Zoom-in on the core of the fault. D.1E: Zoom-in on striated fracture plane (ruler is in centimeters).